



HAL
open science

The SOPHIE search for northern extrasolar planets IX. Populating the brown dwarf desert

P. A. Wilson, G. Hébrard, N. C. Santos, J. Sahlmann, G. Montagnier, N.
Astudillo-Defru, I. Boisse, F. Bouchy, J. Rey, L. Arnold, et al.

► **To cite this version:**

P. A. Wilson, G. Hébrard, N. C. Santos, J. Sahlmann, G. Montagnier, et al.. The SOPHIE search for northern extrasolar planets IX. Populating the brown dwarf desert. *Astronomy & Astrophysics - A&A*, 2016, 588, 10.1051/0004-6361/201527581 . hal-01440109

HAL Id: hal-01440109

<https://hal.science/hal-01440109v1>

Submitted on 4 Jan 2025

HAL is a multi-disciplinary open access archive for the deposit and dissemination of scientific research documents, whether they are published or not. The documents may come from teaching and research institutions in France or abroad, or from public or private research centers.

L'archive ouverte pluridisciplinaire **HAL**, est destinée au dépôt et à la diffusion de documents scientifiques de niveau recherche, publiés ou non, émanant des établissements d'enseignement et de recherche français ou étrangers, des laboratoires publics ou privés.



Distributed under a Creative Commons Attribution 4.0 International License

The SOPHIE search for northern extrasolar planets

IX. Populating the brown dwarf desert^{★,★★}

P. A. Wilson¹, G. Hébrard^{1,2}, N. C. Santos^{3,4}, J. Sahlmann⁵, G. Montagnier^{1,2}, N. Astudillo-Defru^{6,7}, I. Boisse⁸, F. Bouchy⁸, J. Rey⁹, L. Arnold², X. Bonfils^{6,7}, V. Bourrier⁹, B. Courcol⁸, M. Deleuil⁸, X. Delfosse^{6,7}, R. F. Díaz⁹, D. Ehrenreich⁹, T. Forveille^{6,7}, C. Moutou^{8,10}, F. Pepe⁹, A. Santerne³, D. Ségransan⁹, and S. Udry⁹

¹ Institut d'Astrophysique de Paris, UMR 7095 CNRS, Université Pierre & Marie Curie, 98bis boulevard Arago, 75014 Paris, France
e-mail: pwilson@iap.fr

² Observatoire de Haute-Provence, CNRS, Université d'Aix-Marseille, 04870 Saint-Michel-l'Observatoire, France

³ Instituto de Astrofísica e Ciências do Espaço, Universidade do Porto, CAUP, Rua das Estrelas, 4150-762 Porto, Portugal

⁴ Departamento de Física e Astronomia, Faculdade de Ciências, Universidade do Porto, Rua do Campo Alegre, 4169-007 Porto, Portugal

⁵ European Space Agency, European Space Astronomy Centre, PO Box 78, Villanueva de la Canada, 28691 Madrid, Spain

⁶ Univ. Grenoble Alpes, IPAG, 38000 Grenoble, France

⁷ CNRS, IPAG, 38000 Grenoble, France

⁸ Aix Marseille Université, CNRS, LAM (Laboratoire d'Astrophysique de Marseille) UMR 7326, 13388 Marseille, France

⁹ Observatoire de Genève, Université de Genève, 51 Chemin des Maillettes, 1290 Sauverny, Switzerland

¹⁰ Canada-France-Hawaii Telescope Corporation, 65-1238 Mamalahoa Hwy, Kamuela, HI 96743, USA

Received 16 October 2015 / Accepted 4 February 2016

ABSTRACT

Radial velocity planet search surveys of nearby solar-type stars have shown a strong scarcity of brown dwarf companions within ~ 5 AU. There is presently no comprehensive explanation for this lack of brown dwarf companions; therefore, increasing the sample of such objects is crucial to understand their formation and evolution. Based on precise radial velocities obtained using the SOPHIE spectrograph at Observatoire de Haute-Provence we characterise the orbital parameters of 15 companions to solar-type stars and constrain their true mass using astrometric data from the HIPPARCOS space mission. The nine companions not shown to be stellar in nature have minimum masses ranging from ~ 13 to $70 M_{\text{Jup}}$, and are well distributed across the planet/brown dwarf mass regime, making them an important contribution to the known population of massive companions around solar-type stars. We characterise six companions as stellar in nature with masses ranging from a minimum mass of $76 \pm 4 M_{\text{Jup}}$ to a mass of $0.35 \pm 0.03 M_{\odot}$. The orbital parameters of two previously known substellar candidates are improved.

Key words. techniques: radial velocities – stars: general – brown dwarfs

1. Introduction

The upper mass boundary separating brown dwarfs from stars is well defined at the hydrogen burning limit whereby an object with a central temperature insufficient for sustained hydrogen fusion in its core is considered a brown dwarf (Chabrier & Baraffe 1997; Burrows et al. 2001). Without hydrogen fusion in the core, thermal equilibrium is never reached and the brown dwarf steadily cools with time. The boundary between brown dwarfs and planets is currently unclear and is still a subject of much debate. Numerous studies have used the deuterium burning limit as a lower brown dwarf limit whereby an object is no longer able to fuse deuterium in its core. For a solar metallicity object, the lower limit for deuterium burning is $\sim 13 M_{\text{Jup}}$ (Burrows et al. 2001). The deuterium burning limit, however, is dependant on a number of different factors such as the helium abundance, the

initial deuterium abundance, as well as the metallicity of the object (Spiegel et al. 2011). More importantly, there is no robust physical justification for this limit. It has been suggested that the overlapping brown dwarf and planet regimes should be distinguished by their formation mechanisms (Chabrier et al. 2014), with planets forming via core accretion in protostellar discs and brown dwarfs similar to stars which form in molecular clouds.

Differentiating observationally between the two formation scenarios is a challenge owing to the lack of clear observational diagnostics. There are, however, ways of differentiating between the two formation mechanisms such as mean density measurements and the composition of the object (Chabrier et al. 2014). A measured radius which is significantly smaller than expected for a near solar metallicity object can indicate an enhanced abundance of heavy elements in favour of the core accretion scenario. The opposite is not necessarily true as a larger than expected radii does not necessarily mean there is an underabundance of heavy materials (Leconte et al. 2009), but could instead be due to a radius inflation which is observed in many hot-Jupiter atmospheres (Charbonneau et al. 2000; Bodenheimer et al. 2003; Burrows et al. 2007). A larger than expected radius could also be the result of a high-metallicity atmosphere with thick clouds

* Based on observations collected with the SOPHIE spectrograph on the 1.93 m telescope at Observatoire de Haute-Provence (CNRS), France, by the SOPHIE Consortium.

** The radial velocity measurements are only available at the CDS via anonymous ftp to cdsarc.u-strasbg.fr (130.79.128.5) or via <http://cdsarc.u-strasbg.fr/viz-bin/qcat?J/A+A/588/A144>

(Burrows et al. 2011). If the object has formed through disk instabilities we expect to have a chemical composition similar to the original star forming material, whereas if it formed via core accretion it may be enhanced or depleted in some elements. The limiting factor for spectroscopically differentiating between the two scenarios are spectral resolution and signal-to-noise (S/N), which are ultimately governed by the brightness of the object. The high-resolution observations are further limited to young self-luminous objects with wide enough separations from their host star to allow for spectroscopic observations.

The brown dwarf desert is a term used to describe the absence of brown dwarf companions on tight orbits (≤ 5 AU, $P \leq 11$ yr) around solar-mass stars compared to both planetary and stellar mass companions (Marcy & Butler 2000; Marcy et al. 2005; Grether & Lineweaver 2006). The lack of such close-in brown dwarf companions is well established as these objects are readily detected by planet search RV surveys which are most sensitive to massive objects on close-in orbits (Ma & Ge 2014). Within the mass domain that is dominated by planets, the occurrence rate increases with decreasing mass (e.g. Howard et al. 2010; Mayor et al. 2011), whereas for low-mass stellar companions, on the other side of the desert, the occurrence rate increases with increasing mass (Grether & Lineweaver 2006). The sparse number of companions in the brown dwarf mass regime compared to planetary mass companions, free floating brown dwarfs, and the initial mass function of individual stars indicates a separate formation mechanism between the planetary and stellar companions (Chabrier et al. 2014). To test this hypothesis a larger number of objects in the brown dwarf desert are needed.

In this paper we present the detection of 15 companions to solar-type stars straddling the brown dwarf desert. The host star magnitudes range from 7.56 to 9.76 in *V*-band and they are located at a distance of 31.46 to 94.16 pc from Earth. The observations are part of the SOPHIE search for northern extrasolar planets sub-programme 2 (Bouchy et al. 2009) that covers a volume-limited sample of ~ 2000 stars orbiting main-sequence stars of F, G, and K spectral type. The work presented in this paper is a continuation of work by Díaz et al. (2012) who characterised seven new objects with minimum masses between $\sim 10 M_{\text{Jup}}$ and $\sim 90 M_{\text{Jup}}$.

In Sect. 2 we discuss the observations and the data reduction. In Sect. 3 we present the analysis techniques used and the results are presented in Sect. 4. We summarise the results in Sect. 5.

2. SOPHIE radial velocities

2.1. Observations

The observations were conducted using the 1.93 m telescope at the Haute-Provence Observatory (OHP) together with the SOPHIE cross-dispersed échelle spectrograph. The spectrograph, which is kept in a thermally controlled chamber with the dispersive elements kept at a constant pressure in a nitrogen filled chamber, covers the 3872–6943 Å wavelength range, spanning 39 orders (Perruchot et al. 2008). Observations were performed in a high-resolution mode with $\lambda/\Delta\lambda \sim 75\,000$ at 550 nm. ThAr calibrations were obtained approximately every two hours during the night and were used to calculate the wavelength calibration drift. Two fibers were used during the observations, a target fiber and a sky fiber. The sky fiber observations were used to remove the sky background contribution for those situations where the observations are contaminated by moonlight being scattered in Earth's atmosphere. The sky background was removed when deemed significant by a detectable

Table 1. Observations.

Name	Timespan of observations [days]	No. of observations
HD 6664	1577	25
HD 283668	2751	16
BD+73 0275	3282	25
HD 39392	804	15
HD 50761	1472	16
HD 51813	2301	14
HD 56709	2971	25
HD 77065	10 388	106
BD+26 1888	1476	19
HD 122562	2962	29
HD 132032	735	18
HD 134113	10 127	103
HD 134169	382	12
HD 160508	1236	26
BD+24 4697	497	17

cross correlation function (CCF) peak in the sky background fiber data (e.g. Bonomo et al. 2010). A list of the timespan and number of the observations are listed in Table 1.

2.2. Data reduction

The data were reduced using the SOPHIE pipeline (Bouchy et al. 2009) which processes the raw images into wavelength-calibrated two-dimensional spectra. It includes the localisation of the 39 orders followed by an optimal order extraction, cosmic-ray rejection, wavelength correction and spectral flat field corrections. The spectra were subsequently crosscorrelated with numerical cross correlation masks which included the F0, G2 and K5 spectral types. Orders 5 to 38 were used as they produced the smallest scatter on average. The radial velocities, contrast relative to the baseline, the full width at half maximum (FWHM) and the bisector velocity span of the CCF were all calculated using a Gaussian fit to the CCF. The bisector velocity span was calculated using the method described by Queloz et al. (2001). The radial velocity observations obtained after the 17th of June 2011 instrument upgrade (Perruchot et al. 2011), are known as the SOPHIE+ measurements (Bouchy et al. 2013). Courcol et al. (2015) reported on a long-term systematic instrumental drift of the order of a few m/s. This drift was not removed from the data as it has a negligible impact on the RV variations reported in this paper. The radial velocity models presented here take into account any offset between the two observational epochs (before and after the instrument upgrade) by letting the radial velocity offset between each epoch of observations vary independently. This is to account for a systematic offsets which may have been introduced during the instrument upgrade. The average signal-to-noise for all objects is 49 with observations spanning 399 to 2936 days.

3. Analysis

3.1. Stellar parameters

The stellar parameters, temperature, gravity, microturbulence and metallicity were all obtained using the spectroscopic analysis methods described in Santos et al. (2013), and references therein. The method makes use of the equivalent widths of a list of Fe I and Fe II lines, as measured in the SOPHIE spectra. All the analysis is done in LTE using the 2010 version of the MOOG software (Snedden 1973) and one-dimensional

Table 2. Stellar properties.

Name	π [mas]	V	Temperature [K]	$\log g$ [cgs]	v_{micro} [km s ⁻¹]	$\log R'_{\text{HK}}$ [dex]	[Fe/H] [dex]	$v \sin i$ [km s ⁻¹]	Mass M_{\odot}
HD 6664	27.29 ^u	7.78	5854 ± 22	4.53 ± 0.04	0.96 ± 0.03	-4.50 ± 0.10	-0.20 ± 0.02	2.5 ± 1.0	0.92 ± 0.07
HD 283668	23.66	9.44	4845 ± 66	4.35 ± 0.12	0.02 ± 0.30	-5.01 ± 0.10	-0.75 ± 0.12	1.3 ± 1.0	0.68 ± 0.06
BD+73 0275	26.18 ^u	8.98	5260 ± 25	4.43 ± 0.04	–	-4.82 ± 0.10	-0.42 ± 0.02	2.8 ± 1.0	0.77 ± 0.05
HD 39392	10.62	8.38	5951 ± 42	4.08 ± 0.03	1.28 ± 0.06	-5.11 ± 0.16	-0.32 ± 0.03	1.9 ± 1.0	1.08 ± 0.08
HD 50761	11.52	8.13	6450 ± 70	4.47 ± 0.17	1.93 ± 0.12	-5.06 ± 0.18	-0.02 ± 0.05	8.2 ± 1.0	1.19 ± 0.10
HD 51813	15.13 ^u	8.67	6012 ± 32	4.53 ± 0.05	1.24 ± 0.04	-4.60 ± 0.11	0.13 ± 0.02	4.9 ± 1.0	1.06 ± 0.07
HD 56709	14.99	7.56	6926 ± 73	4.63 ± 0.09	1.80 ± 0.11	–	0.03 ± 0.04	5.1 ± 1.0	1.33 ± 0.09
HD 77065	31.52	8.82	4990 ± 100	4.28 ± 0.20	–	-5.01 ± 0.10	-0.51 ± 0.10	2.8 ± 1.0	0.75 ± 0.06
BD+26 1888	26.30	9.76	4748 ± 87	4.3 ± 0.2	0.74 ± 0.24	–	0.02 ± 0.04	2.8 ± 1.0	0.76 ± 0.08
HD 122562	18.60	7.69	4958 ± 67	3.74 ± 0.14	1.05 ± 0.09	-5.27 ± 0.16	0.31 ± 0.04	3.4 ± 1.0	1.13 ± 0.13
HD 132032	17.86	8.11	6035 ± 33	4.45 ± 0.05	1.2 ± 0.04	-5.13 ± 0.22	0.22 ± 0.03	3.2 ± 1.0	1.12 ± 0.08
HD 134113 [†]	13.91	8.26	5782 ± 22	4.25 ± 0.03	1.27 ± 0.04	-5.09 ± 0.23	-0.74 ± 0.02	1.5 ± 1.0	0.81 ± 0.01
HD 134169	17.27	7.70	5940 ± 40	4.33 ± 0.03	–	-5.09 ± 0.14	-0.51 ± 0.10	1.0 ± 1.0	0.91 ± 0.05
HD 160508	10.83	8.11	6212 ± 30	4.16 ± 0.03	1.5 ± 0.04	-5.25 ± 0.13	0.01 ± 0.02	3.7 ± 1.0	1.25 ± 0.08
BD+24 4697	20.51	9.74	5077 ± 32	4.67 ± 0.07	1.04 ± 0.05	-4.69 ± 0.10	-0.11 ± 0.02	1.5 ± 1.0	0.75 ± 0.05

Notes. ^(u) Parallaxes have been updated following the astrometric analysis presented in this paper. ^(†) Values are adopted from (Sousa et al. 2011). Alternate values computed in this study: $T_{\text{eff}} = 5940 \pm 40$ K, $\log g = 4.32 \pm 0.05$, $[\text{Fe}/\text{H}] = -0.70 \pm 0.03$ and $m = 0.89 \pm 0.05 M_{\odot}$.

Kurucz (1993) model atmospheres. The stellar parameters were determined by using excitation and ionisation equilibrium principles, and minimising the correlation between $\log \epsilon(\text{Fe I})$ and χ_I (excitation potential) as well as $\log \epsilon(\text{Fe I})$ and $\log(W_{\lambda}/\lambda)$ making sure the mean abundance between the Fe I and Fe II lines were equivalent.

The aforementioned stellar parameters were subsequently compared to interpolated isochrones by Girardi et al. (2000) using the method described in da Silva et al. (2006). The metallicities were computed using two methods, through the analysis of the spectra and from the CCF using the Boisse et al. (2010) calibration. The metallicities from the spectral analysis were obtained from a detailed analysis of carefully selected lines, which resulted in an typical accuracy of ~ 0.04 dex. The metallicities from the CCF were obtained from a global, empirical calibration and provide a typical accuracy of ~ 0.1 dex. We found that the two methods give consistent results but use the spectral analyses technique for all the targets as the obtained values are more accurate. The largest metallicity difference derived from the two methods was for HD 77065 where there was a 2.6σ discrepancy. For this object we used the spectral analyses method for consistency with the other results. The stellar parameters, including metallicities, are presented in Table 2.

Intrinsic phenomena caused by photospheric features associated with chromospheric activity such as starspots and convective inhomogeneities are known to influence RV measurements up to a few tens of m s^{-1} (e.g. Campbell et al. 1991; Saar & Donahue 1997; Saar et al. 1998; Santos et al. 2000; Boisse et al. 2011). The impact of stellar activity can affect the derived orbital parameters if the RV semi-amplitudes are similar in size to that introduced by stellar noise or when the orbital period is comparable to the rotational period of the host star. Objects with periods longer than ~ 2 years could also be affected by activity cycles or long term variation of the activity level of the star. The objects presented here all have RV amplitudes outside the domain where they might be mistaken for planets when they instead are caused by intrinsic phenomena (e.g. Saar & Donahue 1997). The individual stellar activity values ($\log R'_{\text{HK}}$), reported in Table 2, were obtained following the method of Boisse et al. (2010). The majority of stars in the sample show low activity with only three stars showing an $\log R'_{\text{HK}}$ value larger than -4.7 , namely HD 6664, HD 51813, and BD+24 4697.

3.2. Companion parameters

The parameters of the companions were derived by fitting a single Keplerian orbit model to the radial velocity data. The free parameters were the orbital period P , the eccentricity e , the argument of periapsis ω , the semi-amplitude K , the periastron time T_0 and the RV shift between the pre (γ_{SOPHIE}) and post (γ_{SOPHIE}^+) instrument upgrade. As the radial velocity variations are large compared to the uncertainties on individual radial velocity points, no periodogram analysis was done. The best fit Keplerian orbit model was obtained by using a genetic algorithm to find the starting point for a Levenberg-Marquardt fit. The uncertainties of the individual parameters were calculated using a one million step Markov chain Monte Carlo (MCMC). The MCMC method obtains samples from the posterior distribution of the model parameters.

The 17th of June 2011 instrument upgrade introduced a systematic shift of $\Delta \text{RV} = 0.03 \pm 0.02 \text{ km s}^{-1}$. This value was calculated by taking the weighted mean of the individual RV shifts (γ -values) available for six of the objects with observations done before and after the instrument upgrade (see γ values in Table 3). The observed shifts measured are likely influenced by the airmass of the observations, the spectral type of the star, choice of cross correlation mask and the spectral orders used. The ΔRV value has a negligible impact on the fits, as it is only marginally different from 0. HD 51813 which also has observations before and after the upgrade was not included in the weighted mean as this object exhibited a shift of $\Delta \text{RV} = -1.5 \pm 0.35 \text{ km s}^{-1}$ which was inconsistent compared to the weighted mean of the other six objects. This shift is thought to be due to the lack of pre-upgrade measurements which all occurred within 4 days, a short amount of time when compared to a much longer orbital period of 1437_{-15}^{+11} days. To account for such a large shift, we fix the pre-upgrade γ value for HD 51813 to a new value consistent with the six targets and recalculate the Keplerian parameters. To avoid underestimating the uncertainties for HD 51813 by fixing the RV shift γ , we adopt the global γ uncertainty of 0.02 km s^{-1} , calculated as the standard deviation of individual RV shifts and use this to inflate the uncertainties on the Keplerian parameters for this object. We find that despite having to adjust the pre-upgrade RV shift, a negligible shift in the derived Keplerian parameters

Table 3. Low-mass binary stars and brown dwarf candidates analysed in this study.

Name	Period [day]	Eccentricity	ω [$^{\circ}$]	K [m/s]	T_0 [BJD - 2 400 000]	γ_{SOPHIE} [km s $^{-1}$]	$\gamma_{\text{SOPHIE}}^{\dagger}$ [km s $^{-1}$]	O-C O-C † [m/s]	a [AU]	$m_2 \sin i^{\ddagger}$ [M_{Jup}]
Low-mass binary stars										
HD 6664B	1718 \pm 11	0.289 \pm 0.002	138.9 \pm 0.5	1417 \pm 4	56 227 \pm 2	6.898 \pm 0.009	6.932 \pm 0.007	14.6	7.0	2.80 \pm 0.09
BD+73 0275B	1423.20 \pm 0.14	0.81386 \pm 0.00038	120.62 \pm 0.09	1624.9 \pm 1.3	57 326.15 \pm 0.04	-26.0352 \pm 0.0035	-26.0297 \pm 0.0014	11.3	4.3	2.31 \pm 0.06
HD 50761B	2092 \pm 11	0.377 \pm 0.007	-127.88 $^{+0.48}_{-0.49}$	2022 $^{+23}_{-21}$	57 692 $^{+7}_{-7}$	23.89 \pm 0.01	23.89 \pm 0.01	7.4	7.4	3.5 \pm 0.2
HD 51813B	1437 $^{+11}_{-15}$	0.735 \pm 0.003	-68.8 $^{+0.4}_{-0.7}$	1150 $^{+14}_{-8}$	55 932.3 $^{+0.3}_{-0.6}$	37.07 \pm 0.02	37.104 $^{+0.010}_{-0.009}$	11.2	13.7	2.6 \pm 0.1
HD 56709B	2499.0 \pm 5.6	0.106 \pm 0.006	153 \pm 4	896 \pm 4	56 958 $^{+30}_{-29}$	-22.296 \pm 0.007	-22.278 \pm 0.006	11.4	12.4	4.03 \pm 0.11
HD 134169B	67.8578 \pm 0.0038	0.10300 \pm 0.00053	-5.02 \pm 0.48	4184.9 \pm 2.4	56 243.940 \pm 0.090	18.9395 \pm 0.0017	18.9395 \pm 0.0017	4.0	0.324 \pm 0.008	83 \pm 4
Brown dwarf candidates to solar-type stars with projected masses between 10 and 80 M_{Jup}										
HD 283668b	2558 \pm 8	0.577 \pm 0.011	-94.6 \pm 1.2	1243 $^{+25}_{-24}$	57 401 $^{+9}_{-8}$	67.80 \pm 0.011	67.79 \pm 0.02	10.8	4.7	3.30 \pm 0.11
HD 39392b	394.3 $^{+1.4}_{-1.2}$	0.394 \pm 0.008	-31.9 \pm 1.3	374.2 $^{+2.4}_{-2.3}$	56 322 \pm 1	-64.632 \pm 0.002	-64.632 \pm 0.002	10.0	10.0	1.08 \pm 0.03
HD 77065b †	119.1135 $^{+0.0026}_{-0.0027}$	0.69397 \pm 0.00036	105.972 \pm 0.065	2817.1 \pm 1.6	56 881.239 \pm 0.006	6.3822 \pm 0.0009	6.3822 \pm 0.0009	5.1	0.438 \pm 0.013	41 \pm 2
BD+26 1888b	536.78 \pm 0.25	0.2675 \pm 0.0016	1.3 \pm 0.7	805.1 \pm 1.3	56 548.3 \pm 0.9	-14.8843 \pm 0.0012	-14.8843 \pm 0.0012	4.7	1.19 \pm 0.05	26 \pm 2
HD 122562b	2777 $^{+104}_{-81}$	0.71 \pm 0.01	-53.9 $^{+1.2}_{-1.3}$	445 $^{+12}_{-10}$	55 935 \pm 2	-13.907 $^{+0.007}_{-0.008}$	-13.868 $^{+0.013}_{-0.011}$	8.0	3.5	4.1 \pm 0.2
HD 132032b	274.33 \pm 0.24	0.0844 \pm 0.0024	-0.9 \pm 0.9	1950.7 \pm 2.2	56 238.0 \pm 0.7	-8.118 \pm 0.005	-8.118 \pm 0.005	3.2	0.87 \pm 0.02	70 \pm 4
HD 134113b †	201.680 \pm 0.004	0.891 \pm 0.002	163.0 \pm 0.2	3965 $^{+55}_{-46}$	56 808.54 \pm 0.05	-60.2027 \pm 0.0015	-60.2027 \pm 0.0015	9.7	0.638 \pm 0.010	47 $^{+2}_{-3}$
HD 160508b	178.9049 \pm 0.0074	0.5967 \pm 0.0009	-168.83 \pm 0.13	1825.3 \pm 2.7	55 998.70 \pm 0.03	22.2054 \pm 0.0035	22.2440 \pm 0.0020	11.0	6.9	0.68 \pm 0.02
BD+24 4697b	145.081 \pm 0.016	0.50048 \pm 0.00043	66.35 \pm 0.09	2728.4 \pm 1.6	55 986.042 \pm 0.037	-36.5913 \pm 0.0016	-36.5913 \pm 0.0016	3.5	0.50 \pm 0.08	53 \pm 3

Notes. † These objects contain data from Latham et al. (2002) where HD 77065 is published as G9-42 and HD 134133 as G66-65. ‡ The uncertainties in stellar mass were included in the uncertainty calculation of $m_2 \sin i$.

Table 4. Parameters of the HIPPARCOS astrometric observations.

Name	HIP	S_n	N_{orb}	σ_Λ (mas)	N_{Hip}	$m_{2,\text{max}}$ (M_\odot)
HD 6664	005313	1	0.7	5.2	115	0.46
HD 283668	020834	5	0.4	4.5	44	...
BD+73 0275	024329	5	0.8	7.5	184	0.29
HD 39392	027828	5	2.7	3.7	114	0.37
HD 50761	033542	7	0.7	2.8	91	0.80
HD 51813	033608	5	0.8	3.4	125	0.55
HD 56709	035697	7	0.4	3.4	106	1.08
HD 77065	044259	5	8.1	3.6	49	0.68
BD+26 1888	044387	5	1.4	6.9	49	0.25
HD 122562	068578	5	0.4	4.0	70	...
HD 132032	073128	5	3.2	4.4	84	0.34
HD 134113	074033	5	5.4	3.7	39	16.13
HD 134169	074079	5	13.4	2.9	41	1.03
HD 160508	086394	5	6.3	5.5	163	1.58
BD+24 4697	113698	5	7.7	6.3	196	0.51

Notes. The columns of this table are defined in Sect. 3.4.

is observed (consistent to within 1σ), even for this object which has the largest shift.

The results of the Keplerian fits of the SOPHIE radial velocities are reported in Table 3. The data and their Keplerian fits are plotted in Fig. A.1.

3.3. Bisector analysis

Variations in the bisector velocity span can be caused by two or more stars blended together or stellar activity. Stellar activity, as discussed in Sect. 3.1, is unlikely to be responsible for any large radial velocity variations since the semi-amplitudes measured are much larger than what variation caused by stellar activity. To look for possible blends we looked for trends in bisector velocity span as a function of radial velocity to see if any of the objects could be accompanied by an additional star blended in the CCF (for more details on this technique see Santerne et al. 2015). We calculated the Kendall rank correlation coefficient for all the objects and found no significant correlations with all p -values being greater than 0.10. However, the object which shows the largest amount of scatter, HD 50761 (see Fig. 1), also shows a tentative detection of being a low-mass binary. We looked for secondary peaks in the CCF using a M4 cross correlation mask (Bouchy et al. 2016) but found no clear detections. The lack of clear detections could in part be due to the low S/N (~ 50) of the individual spectra. Furthermore, HD 56709 and HD 50761 are the fastest rotating stars in the sample with $v \sin i > 5 \text{ km s}^{-1}$ which may have broadened the CCF's to an extent where a clear detection is not possible.

3.4. Analysis of the HIPPARCOS astrometry

All stars listed in Table 4 were observed by the HIPPARCOS satellite (Perryman et al. 1997). We used the new HIPPARCOS reduction (van Leeuwen 2007) to search for signatures of orbital motion in the Intermediate Astrometric Data (IAD). The analysis was performed following Sahlmann et al. (2011b), where a detailed description of the method can be found. Using the parameters of the radial velocity orbit of a given star (Table 3), the IAD was fitted with a seven-parameter model, where the free parameters are the inclination i , the longitude of the ascending node Ω , the parallax ϖ , and offsets to the coordinates

($\Delta\alpha^*$, $\Delta\delta$) and proper motions ($\Delta\mu_{\alpha^*}$, $\Delta\mu_\delta$). A two-dimensional grid in i and Ω was searched for its global χ^2 -minimum. The statistical significance of the derived astrometric orbit was determined with a permutation test employing 1000 pseudo orbits. Uncertainties in the solution parameters were derived by Monte Carlo simulations, which also propagate the uncertainties in the RV parameters. This method has proven to be reliable in detecting orbital signatures in the HIPPARCOS IAD (Sahlmann et al. 2011b,a; Díaz et al. 2012; Sahlmann & Fekel 2013).

Table 4 lists the target names and the basic parameters of the HIPPARCOS observations relevant for the astrometric analysis. The solution type S_n indicates the astrometric model adopted by the new reduction. For the standard five-parameter solution it is “5”, whereas it is “7” when the model included proper-motion derivatives of first order to obtain a reasonable fit, which is the case for HD 56709 and HD 50761. The parameter N_{orb} represents the number of orbital periods covered by the HIPPARCOS observation timespan and N_{Hip} is the number of astrometric measurements with a median precision of σ_Λ . The last column in Table 4 shows the maximum companion mass ($m_{2,\text{max}}$) that would be compatible with a non-detection in the HIPPARCOS astrometry. Outliers in the IAD have to be removed because they can substantially alter the outcome of the astrometric analysis. We eliminated one outlier for both HD 160508 and HD 77065.

Even if the astrometric signal is not detected in the astrometric data, i.e. the derived significance is low, we can use the HIPPARCOS observations to set an upper limit to the companion mass by determining the minimum detectable astrometric signal a_{min} of the individual target. When the data cover at least one complete orbit, Sahlmann et al. (2011b,a) have shown that an astrometric signal-to-noise of $S/N \gtrsim 6-7$ is required to obtain a detection at the 3σ level, where $S/N = a \sqrt{N_{\text{Hip}}}/\sigma_\Lambda$ and a is the semi-major axis of the detected orbit. Using a conservative S/N-limit of 8, we derive the upper companion mass limit $m_{2,\text{max}}$ as the companion mass which introduces the astrometric signal

$$a_{\text{min}} = 8 \frac{\sigma_\Lambda}{\sqrt{N_{\text{Hip}}}} (1 - e^2), \quad (1)$$

where the factor $1 - e^2$ accounts for the most unfavourable case of $i = 90^\circ$ and $\Omega = 90^\circ$ in which the astrometric signal is given by the semi-minor axis of the orbit. The last column in Table 4 lists this upper companion mass limit.

4. Results

We characterise the orbital parameters of 15 companions of solar-type stars, 13 of which are newly discovered companions. Their minimum masses $m_2 \sin i$ range from $13.2 M_{\text{Jup}}$ (HD 39392b) to $145 M_{\text{Jup}}$ (HD 50761B). We further improve the parameters of HD 134113 and HD 77065 by combining our new observations with previous observations by Latham et al. (2002). For three stars, we found significant ($>3\sigma$) orbit signatures in the HIPPARCOS IAD. Tentative detections ($1.5 \leq \sigma \leq 3$) were seen for an additional two objects. The largest residual dispersion is found for the most active stars in the sample such as HD 6664 and HD 51813 with the less active stars such as HD 122562, HD 132032 and HD 134169 showing the smallest dispersion.

We divide the objects in this study into low-mass binary stars, low-mass binary stars candidates and brown dwarf candidates and present information concerning each object in the subsections below. The numerical results from astrometry are presented in Tables 5, 6 with the Keplerian fit parameters presented in Table 3. Objects we regard as likely to be stellar in

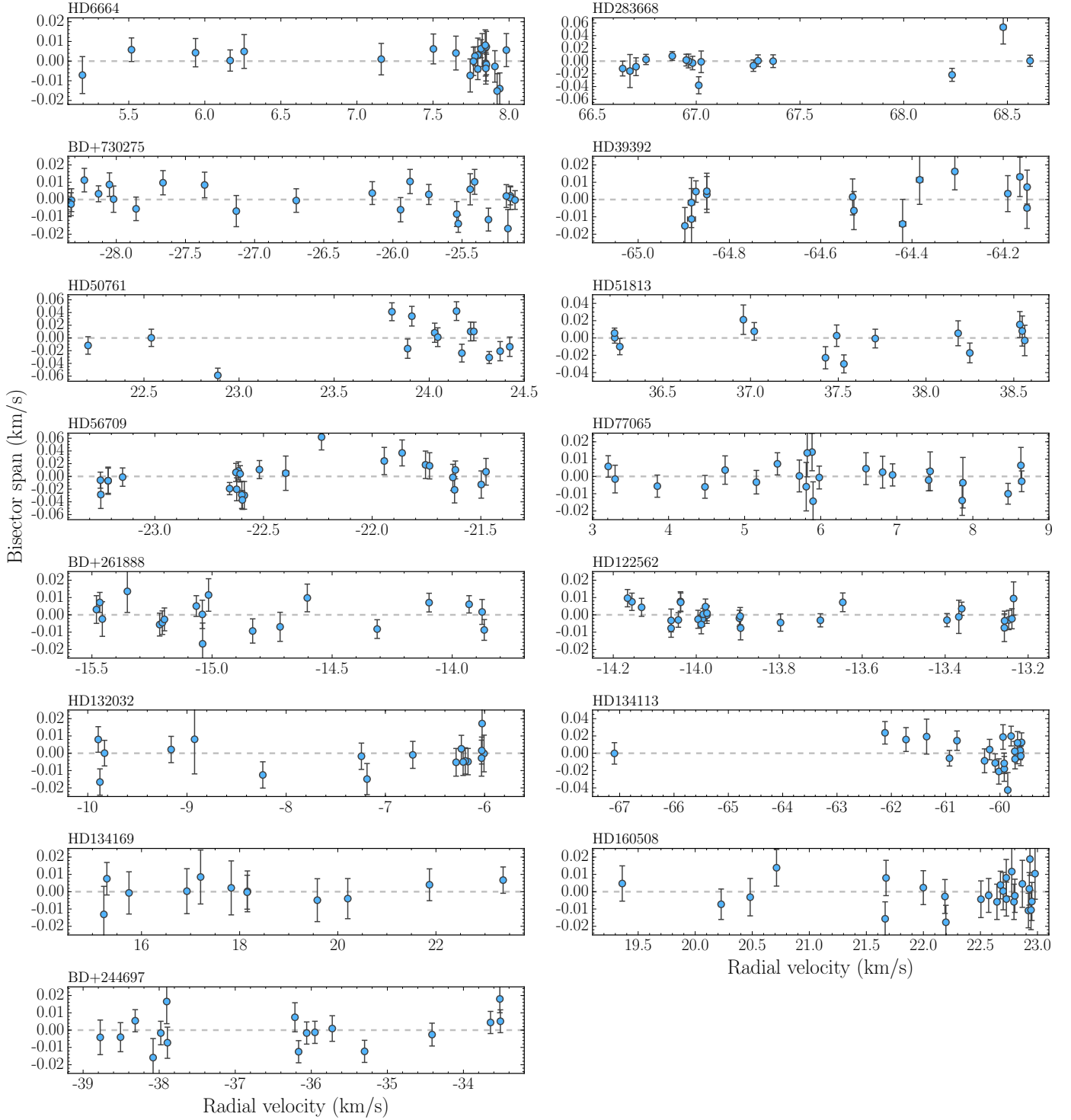


Fig. 1. Bisector span as a function of radial velocity for all the targets in the sample. The dashed line represents a zero bisector span and is shown as a reference.

nature are designated with the stellar name followed by the suffix “B”. Objects with minimum masses below the hydrogen burning limit are designated as brown dwarf candidates with the suffix “b” added to the name of the star. As the parameters improve through continued observations, especially for astrometric observations, these suffixes are likely to change for at least some of the companions which later might turn out to be low-mass stars as their inclination is determined.

4.1. Low-mass binary stars

The mass limit which divides brown dwarfs and stars is $\sim 0.075 M_{\odot}$ (Burrows et al. 1997; Chabrier & Baraffe 2000) (depending on metallicity). We detect the astrometric orbital solution for three low-mass stellar companions with a statistical significance greater than 3σ orbiting HD 6664, BD+730275 and HD 51813. Two additional tentative astrometric detections are

Table 5. Astrometric parameters determined for systems with a significant or tentative astrometric signal in the HIPPARCOS data.

Source	$\Delta\alpha^*$ (mas)	$\Delta\delta$ (mas)	ϖ (mas)	$\Delta\varpi$ (mas)	$\Delta\mu_{\alpha^*}$ (mas yr ⁻¹)	$\Delta\mu_{\delta}$ (mas yr ⁻¹)	i (deg)	Ω (deg)
HD 6664	$-4.3^{+1.8}_{-1.8}$	$-16.9^{+1.5}_{-1.5}$	$27.29^{+0.90}_{-0.91}$	-4.50	$22.6^{+1.8}_{-1.8}$	$-2.9^{+1.5}_{-1.5}$	$165.1^{+1.0}_{-1.2}$	$319.0^{+8.1}_{-8.1}$
HD 56709 ^T	$1.0^{+3.6}_{-3.6}$	$15.6^{+2.6}_{-2.6}$	$15.32^{+1.02}_{-1.02}$	0.34	$-13.7^{+2.0}_{-2.0}$	$0.6^{+3.2}_{-3.2}$	$170.6^{+1.5}_{-2.1}$	$177.4^{+17.7}_{-11.0}$
BD+730275	$7.3^{+5.7}_{-6.2}$	$14.0^{+3.3}_{-3.1}$	$26.18^{+1.06}_{-1.06}$	2.11	$0.4^{+1.4}_{-1.4}$	$-7.8^{+1.8}_{-1.8}$	$14.1^{+2.3}_{-1.7}$	$259.3^{+20.9}_{-23.3}$
HD 51813	$8.9^{+2.1}_{-2.1}$	$7.1^{+4.2}_{-4.0}$	$15.13^{+1.03}_{-1.03}$	-1.00	$-4.8^{+1.3}_{-1.3}$	$-1.9^{+1.0}_{-1.0}$	$169.2^{+2.0}_{-3.2}$	$5.3^{+22.6}_{-23.9}$
HD 50761 ^T	$-5.5^{+3.3}_{-3.1}$	$0.3^{+2.2}_{-2.0}$	$12.06^{+0.77}_{-0.77}$	0.53	$2.3^{+1.8}_{-1.8}$	$7.5^{+1.5}_{-1.5}$	$13.2^{+4.8}_{-2.8}$	$13.9^{+43.6}_{-43.3}$

Notes. ^(T) These objects are regarded as systems with a tentative astrometric signal in the HIPPARCOS data.

Table 6. Solution parameters determined for systems with a significant or tentative astrometric signal in the HIPPARCOS data.

Source	$a \sin i$ (mas)	a (mas)	M_2 (M_{\odot})	M_2 (3σ) (M_{\odot})	a_{rel} (mas)/(AU)	O-C ₅ (mas)	O-C ₇ (mas)	$\chi^2_{7,\text{red}}$	p -value (%)	Significance (%)
HD 6664	6.81	$22.8^{+1.4}_{-1.4}$	$0.35^{+0.03}_{-0.03}$	(0.26, 0.46)	83.0/3.0	7.00	4.03	0.53	1.7×10^{-30}	>99.9
HD 56709 ^{T,a}	3.13	$19.4^{+2.8}_{-2.8}$	$0.54^{+0.12}_{-0.12}$	(0.25, 1.08)	68.4/4.5	4.97	4.27	1.39	1.9×10^{-11}	86.8
BD+730275	2.90	$12.9^{+1.7}_{-1.8}$	$0.20^{+0.03}_{-0.03}$	(0.11, 0.29)	63.7/2.4	8.04	6.81	0.75	2.2×10^{-11}	>99.9
HD 51813	1.66	$8.3^{+1.7}_{-1.7}$	$0.27^{+0.07}_{-0.07}$	(0.10, 0.55)	41.5/2.7	4.28	3.67	0.89	1.1×10^{-5}	>99.9
HD 50761 ^T	1.99	$9.1^{+2.0}_{-2.0}$	$0.38^{+0.11}_{-0.11}$	(0.16, 0.80)	38.5/3.2	3.74	3.00	1.15	2.7×10^{-7}	99.4

Notes. ^(T) These objects are regarded as systems with a tentative astrometric signal in the HIPPARCOS data. ^(a) These parameters correspond to the tentative orbit detection discussed in the text.

made for HD 56709 ($\approx 1.5\sigma$) and HD 50761 (2.7σ). The astrometric analysis yields masses which range from 0.20 to $0.54 M_{\odot}$ (see Table 6). Each companion is described in more detail in the subsections below, which includes the tentative detections. We categorise HD 50761, HD 56709 and HD 134169 as low-mass binaries. In the case of HD 50761 it is because we derive a minimum mass of $m_2 \sin i = 145 \pm 4 M_{\text{Jup}}$. For HD 56709 and HD 134169 it is because their large minimum masses of $m_2 \sin i = 72 \pm 4 M_{\text{Jup}}$ and $m_2 \sin i = 83 \pm 4 M_{\text{Jup}}$ respectively, make them much more likely to be low-mass stars rather than brown dwarfs.

4.1.1. HD 6664

HD 6664 is a G1V star with a mass of $0.92 \pm 0.07 M_{\odot}$. RV measurements show the presence of a companion with an orbital period of 1718 ± 11 days and with a minimum mass of $80 \pm 5 M_{\text{Jup}}$, which by itself would indicate a companion which is stellar in nature. According to Riddle et al. (2015) HD 6664 is a triple system. The astrometric analysis was done on the inner pair. The outer companion at $>26''$ has no influence on the detectability of the inner orbit with HIPPARCOS astrometry and is outside the SOPHIE aperture. We detected the astrometric signal in the HIPPARCOS data with high significance $>3.3\sigma$ ($>99.9\%$) and measured a semi-major axis of $a = 22.8 \pm 1.4$ mas. HD 6664 is the only source in this study with solution type of “1”, which already indicated non-standard astrometric motion. The system’s effective inclination is small (15° out of the sky plane) with an orbital inclination of $i = 165.1^{+1.0}_{-1.2}$ and we measure the longitude of the ascending node of $\Omega = 319.0 \pm 8.1^\circ$. Based on the orbit’s inclination, we determine a companion mass of $M_2 = 0.35 \pm 0.03 M_{\odot}$, i.e. HD 6664 B is indeed a low-mass star.

There is a significant offset in the updated proper motion in RA of $\Delta\mu_{\alpha^*} = 22.6 \pm 1.8$ mas yr⁻¹. More importantly, the new parallax $\varpi = 27.29^{+0.90}_{-0.91}$ mas is significantly smaller (by

-4.5 mas) than the catalogue value of $\varpi_{\text{HIP2}} = 31.8 \pm 1.7$ mas (van Leeuwen 2007), and the revised distance to HD 6664 is 36.6 ± 1.2 pc. The sky-projected orbit of HD 6664 and the HIPPARCOS measurements are shown in Fig. 2.

4.1.2. BD+73 0275

BD+73 0275 is a G5 star with a mass of $0.77 \pm 0.05 M_{\odot}$. RV measurements show the presence of a $m_2 \sin i = 44 \pm 3 M_{\text{Jup}}$ companion on a 1423.20 ± 0.14 day orbit. We detected the HIPPARCOS astrometric orbit of BD+730275 with a significance $>3.3\sigma$ ($>99.9\%$). The orbit’s size and orientation is determined by $i = 14.1^{+2.3}_{-1.7}$ deg, $\Omega = 259.3^{+20.9}_{-23.3}$ deg, and $a = 12.9^{+1.7}_{-1.8}$ mas. The sky-projected orbit of BD+730275 and the HIPPARCOS measurements are shown in Fig. 3. Consequently, we determined the secondary mass to be $M_2 = 0.20 \pm 0.03 M_{\odot}$, i.e. the companion of BD+730275 is a low-mass star. This low-mass star is the only one found within our sample (and that of Díaz et al. 2012) to orbit a star with an effective temperature (5260 ± 25 K) less than the Sun. The companion to BD+73 0275, similar to HD 51813, has a minimum mass within the driest part of the brown dwarf desert before astrometry revealed the companion to be stellar in nature.

4.1.3. HD 50761

HD 50761 is a F8 star with a mass of $1.19 \pm 0.10 M_{\odot}$, the second most massive target in the sample. RV measurements show a companion with an orbital period of 2092 ± 11 days and with a minimum mass of $m_2 \sin i = 145^{+36}_{-29} M_{\text{Jup}}$. HD 50761 is the only object which does not have RV observations spanning an entire orbital period of their companion. This makes the minimum mass estimate difficult to constrain. HD 50761 is the object which shows the largest amount of scatter in the bisector

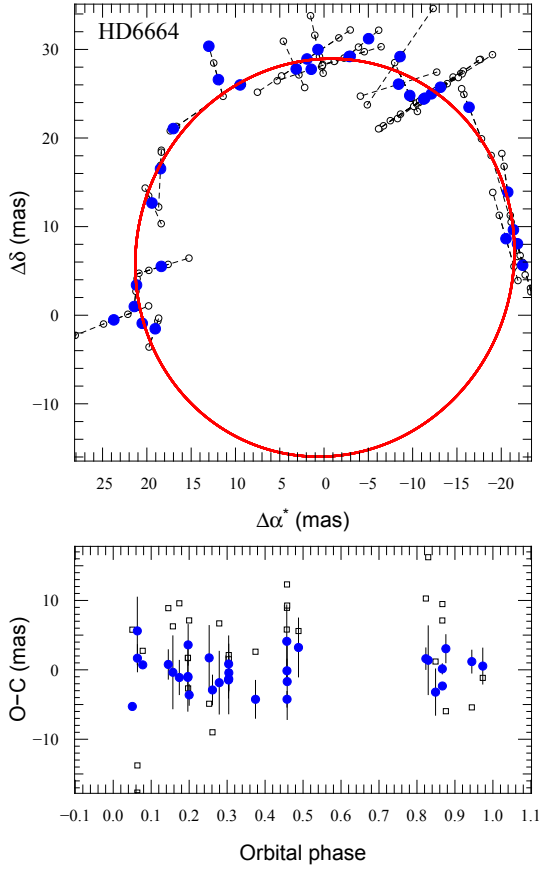


Fig. 2. *Top:* astrometric orbit of HD 6664 projected on the sky. North is up and east is left. The solid red line shows the orbital solution, which is orientated clockwise, and open circles mark the individual HIPPARCOS measurements. The dashed lines represents the scan angle which connects these one-dimensional position measurements. The blue filled circles are the mean of the HIPPARCOS measurements obtained during one orbit. *Bottom:* O–C residuals for the normal points of the orbital solution (filled blue circles) and of the five-parameter model without companion (open squares).

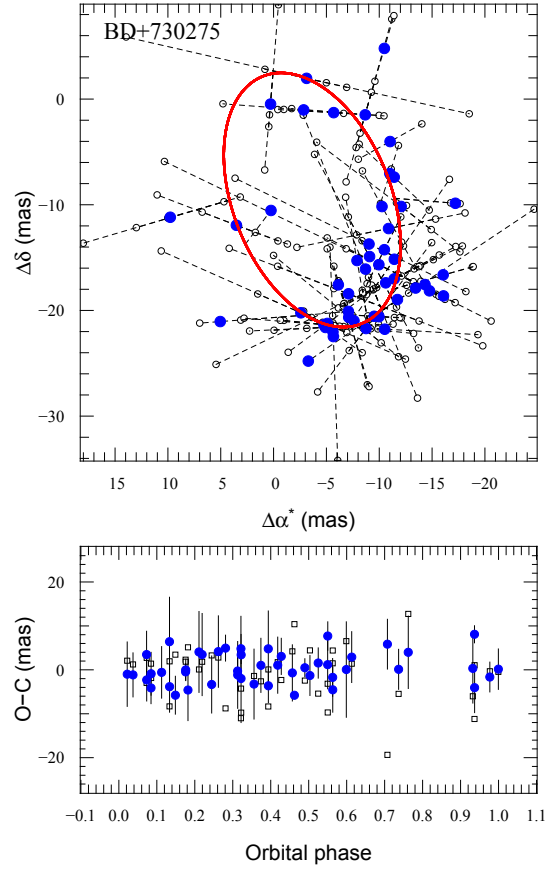


Fig. 3. Astrometric orbit of BD+730275 projected on the sky, cf. Fig. 2, corresponding to one set of RV parameters. The star’s motion is counter-clockwise.

span (see Fig. 1). No clear secondary peaks in the CCF were detected using a M4 cross correlation mask. This may be caused by the fast rotation of the star ($8.2 \pm 1.0 \text{ km s}^{-1}$).

We detected the astrometric orbit with HIPPARCOS at 2.7σ significance (99.4%). However, the orbit orientation in the sky given by the angle Ω is poorly constrained by the astrometry. As a consequence, the best-fit astrometric parameters are strongly correlated with parameters derived from RV measurements, e.g. the period P and the periastron time T_0 . In our analysis, we vary those within the quoted uncertainties by randomly drawing 100 sets of RV parameters, thus we obtain 100 clearly different solutions in terms of inclination and Ω . This is illustrated in Fig. 4, where a large variation in the best-fit Ω can be seen. A large range of Ω values is acceptable for different sets of RV parameters, thus the final global distribution is particularly broad and its average value is ill-defined ($\Omega = 13.9^{+43.6}_{-43.3}^\circ$).

This does not affect the significance of the astrometric orbit and the parameters listed in Tables 5 and 6 which naturally account for the correlations, i.e. the uncertainty of the orbital inclination $i = 13.2^{+4.8}_{-2.8}^\circ$ reflects the variation seen in Fig. 4. However,

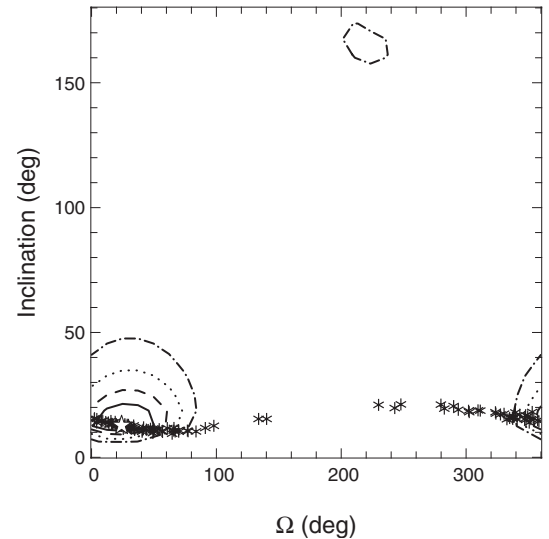


Fig. 4. Joint confidence contours on the i – Ω -grid for one set of spectroscopic parameters of HD 50761. The contour lines correspond to confidences at 1σ (solid), 2σ (dashed), 3σ (dotted), and 4σ (dash-dotted) level. The crosses indicate the position of the best non-linear adjustment solution for each of the 100 Monte Carlo samples of spectroscopic parameters and the star corresponds to the orbit shown in Fig. 5.

it forces us to choose one single set of RV parameters to show one realisation of the astrometric orbit in Fig. 5.

The measured semi-major axis of HD 50761 is $a = 9.1 \pm 2.0 \text{ mas}$ and we determine a companion mass of $M_2 = 0.38 \pm 0.11 M_\odot$, i.e. HD 50761 B is a low-mass star. The large

¹ The global distribution contains 100 000 data points because for each of the 100 RV parameter sets, we run the astrometric analysis 1000 times, see Sahlmann et al. (2011b).

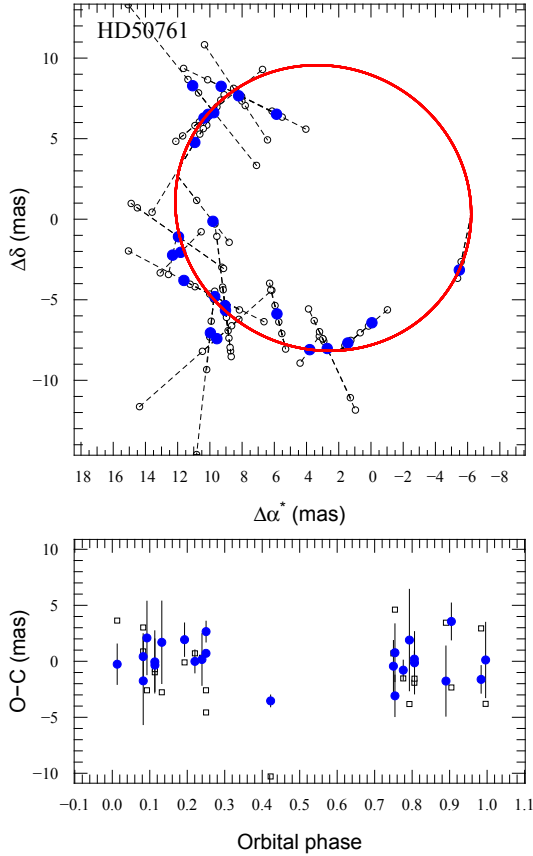


Fig. 5. Astrometric orbit of HD 50761 projected on the sky, cf. Fig. 2, corresponding to one set of RV parameters. The star’s motion is counter-clockwise.

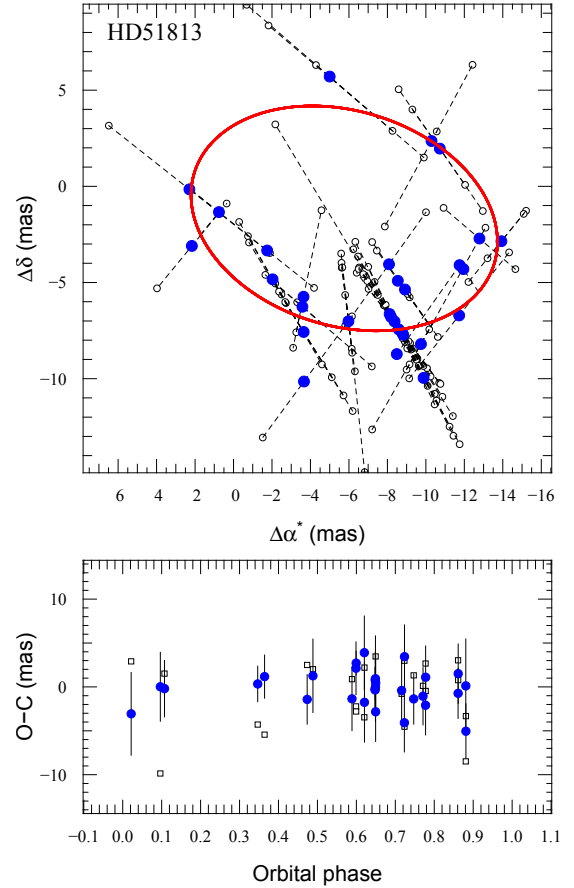


Fig. 6. Astrometric orbit of HD 51813 projected on the sky, cf. Fig. 2. The star’s motion is clockwise.

uncertainty in companion mass reflects the parameter correlations and the ill-defined orbit orientation Ω of the astrometric analysis.

4.1.4. HD 51813

HD 51813 is an active ($\log R'_{\text{HK}} = -4.60 \pm 0.10$) G-type star with a mass of $1.06 \pm 0.07 M_{\odot}$. The stellar activity is likely the cause of the large dispersion seen in the residuals (see Fig. A.1). This is evident when looking at the SOPHIE observations done after the instrument upgrade which typically show a residual dispersion 4–6 times smaller. RV measurements reveal a $m_2 \sin i = 46 \pm 4 M_{\text{Jup}}$ companion on a 1437^{+11}_{-15} day orbit. With only three pre instrument upgrade observations of HD 51813 taken in close succession, the gamma value was adjusted as described in Sect. 3.2. We detected the astrometric orbit with HIPPARCOS with a significance $>3.3\sigma$ ($>99.9\%$) and measured $\Omega = 5.3^{+22.6}_{-23.9} \text{ }^{\circ}$ and $i = 169.2^{+2.0}_{-3.2} \text{ }^{\circ}$. The corresponding semi-major axis of HD 51813 is $a = 8.3 \pm 1.7$ mas and we determined a companion mass of $M_2 = 0.27 \pm 0.07 M_{\odot}$, i.e. HD 51813 B is a low-mass star. The astrometric orbit is shown in Fig. 6. HD 51813, similar to BD+73 0275, has a minimum mass within the driest part of the brown dwarf desert before astrometry revealed the companion to be stellar in nature.

4.1.5. HD 56709

HD 56709 is a F5 star with a mass of $1.33 \pm 0.09 M_{\odot}$, the most massive target in the sample. RV measurements show a companion with an orbital period of 2499.0 ± 5.6 days and with

a minimum mass of $m_2 \sin i = 72 \pm 4 M_{\text{Jup}}$. No clear secondary peaks in the CCF were detected using a M4 cross correlation mask. Astrometry shows a tentative detection of a stellar companion with a permutation significance of only 86.8% ($\approx 1.5\sigma$), which is below our detection threshold. There are however, several indications that the orbit is well constrained by HIPPARCOS astrometry. First, significant acceleration was detected by HIPPARCOS alone, assigning this source a solution type of “7” (van Leeuwen 2007). Second, our F-test asserts at high confidence that the orbital solution of HD 56709 is a much better fit than the standard model (the p -value for the simpler model to be true given in Table 6 is $1.9 \times 10^{-11} \%$), which is supported by a decrease in residual r.m.s. from $O-C_5 = 4.97$ mas to $O-C_7 = 4.27$ mas when including the orbital motion. On the other hand, only $\sim 40 \%$ of the orbit is covered by HIPPARCOS measurements.

We thus claim a tentative detection of the orbit and determine the system parameters, keeping in mind that these may have to be revised when better astrometry becomes available. The semi-major axis is 19.4 ± 2.8 mas. The orbital inclination of $i = 170.6^{+1.5}_{-2.1} \text{ }^{\circ}$ and the companion mass is $M_2 = 0.54 \pm 0.12 M_{\odot}$. The sky-projected orbit of HD 56709 is shown in Fig. 7. Despite being fairly massive, the companion was not detected with speckle interferometry (Mason et al. 2001).

4.1.6. HD 134169

HD 134169 is a F8 star with a mass of $1.19 \pm 0.10 M_{\odot}$. RV measurements show a companion with an orbital period of 67.8578 ± 0.0038 days which is the shortest orbital period amongst the

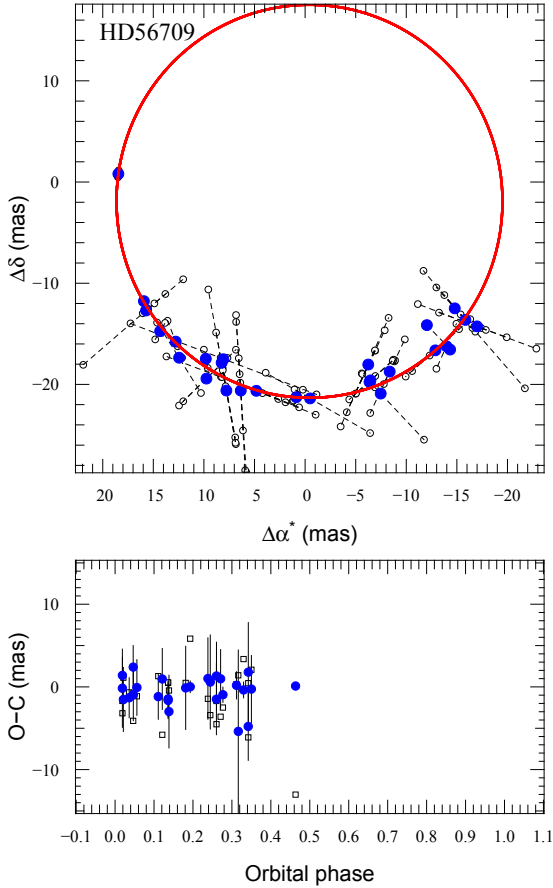


Fig. 7. Astrometric orbit of HD 56709 projected on the sky, cf. Fig. 2. The star’s motion is clockwise.

objects in our sample. The detected companion has a minimum mass of $83 \pm 4 M_{\text{Jup}}$ shown by RV measurements and is therefore likely a stellar companion. HIPPARCOS measurements provide an upper limit on the companion at $1.03 M_{\odot}$. This limit is likely too conservative as a companion with this mass would likely be detected by the bisector analysis described in Sect. 3.3.

4.2. Brown dwarf candidates

In the next subsections we describe the brown dwarf candidates in more detail. A list of brown dwarf candidates to solar-type stars with (projected) masses between 10 and $80 M_{\text{Jup}}$ and periods $< 10^5$ days currently found in literature is presented in Table A.1. The brown dwarf candidates from this study together with the objects from literature are shown in Fig. 8.

4.2.1. HD 283668

HD 283668 is a K3V star which has both got the lowest mass ($0.68 \pm 0.06 M_{\odot}$) as well as the lowest metallicity ($[\text{Fe}/\text{H}] = -0.75 \pm 0.12$) amongst the star in our sample. The detected companion has a minimum mass of $53 \pm 4 M_{\text{Jup}}$ and a period of 2558 ± 8 days.

4.2.2. HD 39392

HD 39392 is a F8 star with a mass of $1.08 \pm 0.08 M_{\odot}$. The star is host to the lowest minimum mass companion at $m_2 \sin i = 13.2 \pm 0.8 M_{\text{Jup}}$ which orbits the star every $394.3_{-1.2}^{+1.4}$ days.

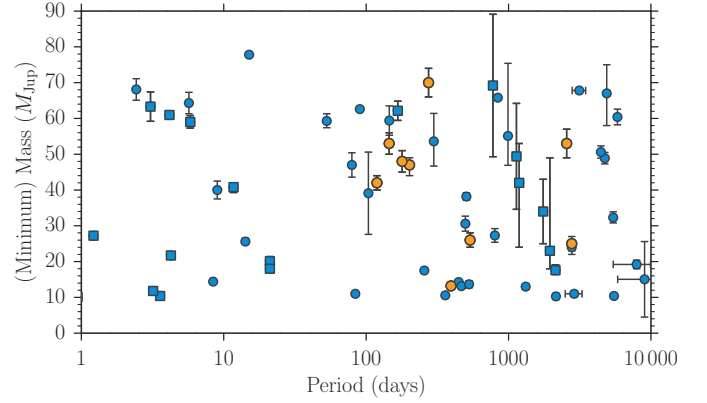


Fig. 8. The minimum mass as a function of orbital period. The data from this study are shown as orange points. The blue points represent data from the literature and are presented in Table A.1. Objects with known masses are indicated using square symbols and objects with minimum mass measurements are shown as round points. All objects have $10 M_{\text{Jup}} \leq m \sin i \leq 80 M_{\text{Jup}}$ and a Period $< 10^5$ days with a host star mass $0.7 M_{\odot} \leq M \leq 1.5 M_{\odot}$.

HIPPARCOS measurements provide an upper limit on the companion at $0.37 M_{\odot}$.

4.2.3. HD 77065

HD 77065 is a G star with a mass of $0.75 \pm 0.06 M_{\odot}$. The detected companion has a minimum mass of $m_2 \sin i = 41 \pm 2 M_{\text{Jup}}$ and an orbit lasting $119.1135_{-0.0027}^{+0.0026}$ days. HD 77065 has the most well constrained orbital parameters of all the objects in the sample due to the number of data points measured. HD 77065 was first reported in Latham et al. (2002) as G9-42. Here we improve the reported parameters with additional data thereby reducing P by 1%, K by 14%, e by 16% and increasing the minimum mass by 2%. HIPPARCOS measurements provide an upper limit on the companion at $0.68 M_{\odot}$. This limit is likely too conservative as a companion with this mass would likely be detected by the bisector analysis described in Sect. 3.3.

4.2.4. BD+26 1888

BD+26 1888 is K7 star with a mass of $0.76 \pm 0.08 M_{\odot}$ and is the coolest star in the sample with $T_{\text{eff}} = 4748 \pm 87$. The $m_2 \sin i = 26 \pm 2 M_{\text{Jup}}$ companion orbits the star with a period of 536.78 ± 0.25 days. HIPPARCOS measurements provide an upper limit on the companion at $0.25 M_{\odot}$.

4.2.5. HD 122562

HD 122562 is a G5 star with a mass of $1.13 \pm 0.13 M_{\odot}$. The companions is found to have a mass of $m_2 \sin i = 24 \pm 2 M_{\text{Jup}}$ and has the longest period orbit with $P = 2777_{-81}^{+104}$ days. HD 122562 is also the least active star in the sample with $\log R'_{\text{HK}} = -5.27 \pm 0.16$ dex and shows the smallest dispersion in the residuals from the Keplerian fit.

4.2.6. HD 132032

HD 132032 is a G5 star with a mass of $1.12 \pm 0.08 M_{\odot}$. The companions is found to have a mass of $m_2 \sin i = 70 \pm 4 M_{\text{Jup}}$ and to orbit the host with a period of 274.33 ± 0.024 days. The high companion mass results in a 50% chance that the true companion

mass is in the stellar regime. HIPPARCOS measurements provide an upper limit on the companion at $0.34 M_{\odot}$.

4.2.7. HD 134113

HD 134113 is a F6/F7V-type star with a mass of $0.81 \pm 0.01 M_{\odot}$. The companion is found to have a mass of $m_2 \sin i = 47_{-3}^{+2} M_{\text{Jup}}$ and to orbit the host with a period of 201.680 ± 0.004 days. HD 134113 was first reported in Latham et al. (2002) as G66-65. Here we improve the reported parameters by $\Delta P = -0.035$ days, $\Delta K = -315$ m/s, $\Delta e = -0.009$. The minimum mass is found to be the same as that of Latham et al. (2002) at $45 M_{\text{Jup}}$. HIPPARCOS measurements provide an upper limit on the companion at $16.13 M_{\odot}$. This upper mass limit can confidently be ruled out by the bisector analysis described in Sect. 3.3.

4.2.8. HD 160508

HD 160508 is a F8V-type star with a mass of $1.25 \pm 0.08 M_{\odot}$. The detected companion has a minimum mass of $m_2 \sin i = 48 \pm 3 M_{\text{Jup}}$ and orbits the star every 178.9049 ± 0.0074 days. HIPPARCOS measurements provide an upper limit on the companion at $1.58 M_{\odot}$. This limit is likely too conservative as a companion with this mass would likely be detected by the bisector analysis described in Sect. 3.3.

4.2.9. BD+24 4697

HD 160508 is a K2-type star with a mass of $0.75 \pm 0.05 M_{\odot}$. The detected companion has a minimum mass of $m_2 \sin i = 53 \pm 3 M_{\text{Jup}}$ and orbits the star every 145.081 ± 0.016 days. HIPPARCOS measurements provide an upper limit on the companion at $0.51 M_{\odot}$.

5. Conclusions

We characterise the orbital parameters of 15 companions to solar-type stars based on observations done with the SOPHIE spectrograph at the Haute-Provence Observatory. Using data from the HIPPARCOS satellite we constrain the true masses of all but two objects. Six companions are regarded as stellar in nature with masses ranging from a minimum mass of $76 \pm 4 M_{\text{Jup}}$ to a mass of $0.35 \pm 0.03 M_{\odot}$. The nine remaining companions that are not shown to be stellar are well distributed across the brown dwarf desert with minimum masses ranging from 13.2 to $70 M_{\text{Jup}}$. Seven of the nine objects are reported for the first time and mark a significant contribution to the number of objects in the brown dwarf desert. The increase in the number of brown dwarf desert objects is an important step required to form a significant statistical sample, which is necessary to be able to understand the formation and subsequent evolution of such objects.

Future characterisation of larger bias-corrected samples of high-mass planets and brown dwarf companions to solar-type stars, confirmed through astrometric observations, are both welcome and required in order to draw sound conclusions on the relationship between the orbital parameters in a quantifiable way. Not until the completion of the SOPHIE search for northern extrasolar planets sub-programme will we be able to derive the fraction of brown dwarfs within the SOPHIE sample. Continued observation will help constrain the different formation scenarios which could provide a way to discern exoplanets from brown dwarfs in the mass region where they overlap.

Acknowledgements. This work is based on observations made with the 1.93 m telescope at the Haute-Provence Observatory. P.A.W. acknowledges the support of the French Agence Nationale de la Recherche (ANR), under program ANR-12-BS05-0012 “Exo-Atmos”. This work was supported by Fundação para a Ciência e a Tecnologia (FCT) through the research grant UID/FIS/04434/2013. N.C.S. and A.S. acknowledge the support by the European Research Council/European Community under the FP7 through Starting Grant agreement number 239953 and support from Fundação para a Ciência e a Tecnologia (FCT, Portugal) in the form of grants reference SFRH/BPD/70574/2010 and PTDC/FIS-AST/1526/2014. N.C.S. also acknowledges the support from in the form of grant reference PTDC/CTE-AST/098528/2008 and through Investigador FCT contract of reference IF/00169/2012 as well as POPH/FSE (EC) by FEDER funding through the program “Programa Operacional de Factores de Competitividade – COMPETE”. A.S. is supported by the European Union under a Marie Curie Intra-European Fellowship for Career Development with reference FP7-PEOPLE-2013-IEF, number 627202. J.S. is supported by an ESA Research Fellowship in Space Science.

References

- Anderson, D. R., Collier Cameron, A., Hellier, C., et al. 2011, *ApJ*, **726**, L19
 Bakos, G. Á., Howard, A. W., Noyes, R. W., et al. 2009, *ApJ*, **707**, 446
 Benedict, G. F., McArthur, B. E., Bean, J. L., et al. 2010, *AJ*, **139**, 1844
 Bodenheimer, P., Laughlin, G., & Lin, D. N. C. 2003, *ApJ*, **592**, 555
 Boisse, I., Eggenberger, A., Santos, N. C., et al. 2010, *A&A*, **523**, A88
 Boisse, I., Bouchy, F., Hébrard, G., et al. 2011, *A&A*, **528**, A4
 Bonomo, A. S., Santerne, A., Alonso, R., et al. 2010, *A&A*, **520**, A65
 Bonomo, A. S., Sozzetti, A., Santerne, A., et al. 2015, *A&A*, **575**, A85
 Borucki, W. J., Koch, D. G., Basri, G., et al. 2011, *ApJ*, **736**, 19
 Bouchy, F., Hébrard, G., Udry, S., et al. 2009, *A&A*, **505**, 853
 Bouchy, F., Bonomo, A. S., Santerne, A., et al. 2011a, *A&A*, **533**, A83
 Bouchy, F., Deleuil, M., Guillot, T., et al. 2011b, *A&A*, **525**, A68
 Bouchy, F., Díaz, R. F., Hébrard, G., et al. 2013, *A&A*, **549**, A49
 Bouchy, F., Ségransan, D., Díaz, R. F., et al. 2016, *A&A*, **585**, A46
 Burrows, A., Marley, M., Hubbard, W. B., et al. 1997, *ApJ*, **491**, 856
 Burrows, A., Hubbard, W. B., Lunine, J. I., & Liebert, J. 2001, *Rev. Mod. Phys.*, **73**, 719
 Burrows, A., Hubeny, I., Budaj, J., Knutson, H. A., & Charbonneau, D. 2007, *ApJ*, **668**, L171
 Burrows, A., Heng, K., & Nampaisarn, T. 2011, *ApJ*, **736**, 47
 Butler, R. P., Wright, J. T., Marcy, G. W., et al. 2006, *ApJ*, **646**, 505
 Campbell, B., Yang, S., Irwin, A. W., & Walker, G. A. H. 1991, in *Bioastronomy: The Search for Extraterrestrial Life – The Exploration Broadens*, eds. J. Heidmann, & M. J. Klein (Berlin: Springer Verlag), *Lect. Notes Phys.*, **390**, 19
 Chabrier, G., & Baraffe, I. 1997, *A&A*, **327**, 1039
 Chabrier, G., & Baraffe, I. 2000, *ARA&A*, **38**, 337
 Chabrier, G., Johansen, A., Janson, M., & Rafikov, R. 2014, *Protostars and Planets VI*, 619
 Charbonneau, D., Brown, T. M., Latham, D. W., & Mayor, M. 2000, *ApJ*, **529**, L45
 Correia, A. C. M., Udry, S., Mayor, M., et al. 2005, *A&A*, **440**, 751
 Courcol, B., Bouchy, F., Pepe, F., et al. 2015, *A&A*, **581**, A38
 Csizmadia, S., Hatzes, A., Gandolfi, D., et al. 2015, *A&A*, **584**, A13
 da Silva, R., Udry, S., Bouchy, F., et al. 2006, *A&A*, **446**, 717
 Deleuil, M., Deeg, H. J., Alonso, R., et al. 2008, *A&A*, **491**, 889
 Díaz, R. F., Santerne, A., Sahlmann, J., et al. 2012, *A&A*, **538**, A113
 Díaz, R. F., Damiani, C., Deleuil, M., et al. 2013, *A&A*, **551**, L9
 Duquennoy, A., & Mayor, M. 1991, *A&A*, **248**, 485
 Endl, M., Hatzes, A. P., Cochran, W. D., et al. 2004, *ApJ*, **611**, 1121
 Feroz, F., Balan, S. T., & Hobson, M. P. 2011, *MNRAS*, **416**, L104
 Fischer, D. A., Marcy, G. W., Butler, R. P., et al. 2002, *PASP*, **114**, 529
 Fischer, D. A., Marcy, G. W., Butler, R. P., et al. 2003, *ApJ*, **586**, 1394
 Fleming, S. W., Ge, J., Mahadevan, S., et al. 2010, *ApJ*, **718**, 1186
 Fleming, S. W., Ge, J., Barnes, R., et al. 2012, *AJ*, **144**, 72
 Ford, E. B., Rowe, J. F., Fabrycky, D. C., et al. 2011, *ApJS*, **197**, 2
 Girardi, L., Bressan, A., Bertelli, G., & Chiosi, C. 2000, *A&AS*, **141**, 371
 Grether, D., & Lineweaver, C. H. 2006, *ApJ*, **640**, 1051
 Halbwachs, J. L., Arenou, F., Mayor, M., Udry, S., & Queloz, D. 2000, *A&A*, **355**, 581
 Haywood, M. 2008, *A&A*, **482**, 673
 Hébrard, G., Bouchy, F., Pont, F., et al. 2008, *A&A*, **488**, 763
 Hellier, C., Anderson, D. R., Collier Cameron, A., et al. 2009, *Nature*, **460**, 1098
 Howard, A. W., Marcy, G. W., Johnson, J. A., et al. 2010, *Science*, **330**, 653
 Jenkins, J. S., Jones, H. R. A., Goździewski, K., et al. 2009, *MNRAS*, **398**, 911
 Jiang, P., Ge, J., Cargile, P., et al. 2013, *AJ*, **146**, 65
 Johns-Krull, C. M., McCullough, P. R., Burke, C. J., et al. 2008, *ApJ*, **677**, 657

- Johnson, J. A., Clanton, C., Howard, A. W., et al. 2011, *ApJS*, 197, 26
- Kane, S. R., Mahadevan, S., Cochran, W. D., et al. 2009, *ApJ*, 692, 290
- Kane, S. R., Henry, G. W., Dragomir, D., et al. 2011a, *ApJ*, 735, L41
- Kane, S. R., Howard, A. W., Pilyavsky, G., et al. 2011b, *ApJ*, 733, 28
- Kurucz, R. 1993, ATLAS9 Stellar Atmosphere Programs and 2 km s⁻¹ grid, Kurucz CD-ROM No. 13 (Cambridge, Mass.: Smithsonian Astrophysical Observatory)
- Latham, D. W., Stefanik, R. P., Mazeh, T., Mayor, M., & Burki, G. 1989, *Nature*, 339, 38
- Latham, D. W., Stefanik, R. P., Torres, G., et al. 2002, *AJ*, 124, 1144
- Leconte, J., Baraffe, I., Chabrier, G., Barman, T., & Levrard, B. 2009, *A&A*, 506, 385
- Ma, B., & Ge, J. 2014, *MNRAS*, 439, 2781
- Ma, B., Ge, J., Barnes, R., et al. 2013, *AJ*, 145, 20
- Marcy, G. W., & Butler, R. P. 2000, *PASP*, 112, 137
- Marcy, G. W., Butler, R. P., Vogt, S. S., et al. 2001, *ApJ*, 555, 418
- Marcy, G., Butler, R. P., Fischer, D., et al. 2005, *Progress of Theoretical Physics Supplement*, 158, 24
- Marmier, M., Ségransan, D., Udry, S., et al. 2013, *A&A*, 551, A90
- Martoli, E., McArthur, B. E., Benedict, G. F., et al. 2010, *ApJ*, 708, 625
- Mason, B. D., Hartkopf, W. I., Holdenried, E. R., & Rafferty, T. J. 2001, *AJ*, 121, 3224
- Mayor, M., Marmier, M., Lovis, C., et al. 2011 [[arXiv:1109.2497](https://arxiv.org/abs/1109.2497)]
- Moutou, C., Mayor, M., Lo Curto, G., et al. 2009, *A&A*, 496, 513
- Moutou, C., Mayor, M., Lo Curto, G., et al. 2011, *A&A*, 527, A63
- Moutou, C., Bonomo, A. S., Bruno, G., et al. 2013, *A&A*, 558, L6
- Nidever, D. L., Marcy, G. W., Butler, R. P., Fischer, D. A., & Vogt, S. S. 2002, *ApJS*, 141, 503
- Parviainen, H., Gandolfi, D., Deleuil, M., et al. 2014, *A&A*, 562, A140
- Patel, S. G., Vogt, S. S., Marcy, G. W., et al. 2007, *ApJ*, 665, 744
- Perrier, C., Sivan, J.-P., Naef, D., et al. 2003, *A&A*, 410, 1039
- Perruchot, S., Kohler, D., Bouchy, F., et al. 2008, in *SPIE Conf. Ser.*, 7014, 70140J
- Perruchot, S., Bouchy, F., Chazelas, B., et al. 2011, in *SPIE Conf. Ser.*, 8151, 15
- Perryman, M. A. C., Lindgren, L., Kovalevsky, J., et al. 1997, *A&A*, 323, L49
- Pilyavsky, G., Mahadevan, S., Kane, S. R., et al. 2011, *ApJ*, 743, 162
- Queloz, D., Henry, G. W., Sivan, J. P., et al. 2001, *A&A*, 379, 279
- Ranc, C., Cassan, A., Albrow, M. D., et al. 2015, *A&A*, 580, A125
- Reffert, S., & Quirrenbach, A. 2006, *A&A*, 449, 699
- Riddle, R. L., Tokovinin, A., Mason, B. D., et al. 2015, *ApJ*, 799, 4
- Saar, S. H., & Donahue, R. A. 1997, *ApJ*, 485, 319
- Saar, S. H., Butler, R. P., & Marcy, G. W. 1998, *ApJ*, 498, L153
- Sahlmann, J., & Fekel, F. C. 2013, *A&A*, 556, A145
- Sahlmann, J., Lovis, C., Queloz, D., & Ségransan, D. 2011a, *A&A*, 528, L8
- Sahlmann, J., Ségransan, D., Queloz, D., et al. 2011b, *A&A*, 525, A95
- Santerne, A., Díaz, R. F., Almenara, J.-M., et al. 2015, *MNRAS*, 451, 2337
- Santos, N. C., Mayor, M., Naef, D., et al. 2000, *A&A*, 361, 265
- Santos, N. C., Israelian, G., Mayor, M., et al. 2005, *A&A*, 437, 1127
- Santos, N. C., Mayor, M., Benz, W., et al. 2010, *A&A*, 512, A47
- Santos, N. C., Sousa, S. G., Mortier, A., et al. 2013, *A&A*, 556, A150
- Sato, B., Fischer, D. A., Ida, S., et al. 2009, *ApJ*, 703, 671
- Sivan, J.-P., Mayor, M., Naef, D., et al. 2004, in *Planetary Systems in the Universe*, ed. A. Penny, *IAU Symp.*, 202, 124
- Siverd, R. J., Beatty, T. G., Pepper, J., et al. 2012, *ApJ*, 761, 123
- Snedden, C. A. 1973, Ph.D. Thesis, The University of Texas at Austin
- Sousa, S. G., Santos, N. C., Israelian, G., et al. 2011, *A&A*, 526, A99
- Southworth, J., Bruni, I., Mancini, L., & Gregorio, J. 2012, *MNRAS*, 420, 2580
- Sozzetti, A., & Desidera, S. 2010, *A&A*, 509, A103
- Spiegel, D. S., Burrows, A., & Milsom, J. A. 2011, *ApJ*, 727, 57
- Tamuz, O., Ségransan, D., Udry, S., et al. 2008, *A&A*, 480, L33
- Triaud, A. H. M. J., Collier Cameron, A., Queloz, D., et al. 2010, *A&A*, 524, A25
- Udry, S., Mayor, M., Naef, D., et al. 2002, *A&A*, 390, 267
- Valenti, J. A., & Fischer, D. A. 2005, *ApJS*, 159, 141
- van Leeuwen, F. 2007, *Hipparcos, the New Reduction of the Raw Data*, Astrophysics and Space Science Library, 350
- Winn, J. N., Holman, M. J., Torres, G., et al. 2008, *ApJ*, 683, 1076
- Winn, J. N., Johnson, J. A., Fabrycky, D., et al. 2009, *ApJ*, 700, 302
- Winn, J. N., Johnson, J. A., Howard, A. W., et al. 2010, *ApJ*, 718, 575
- Wittenmyer, R. A., Endl, M., Cochran, W. D., Levison, H. F., & Henry, G. W. 2009a, *ApJS*, 182, 97
- Wittenmyer, R. A., Endl, M., Cochran, W. D., et al. 2009b, *AJ*, 137, 3529
- Wright, J. T., Upadhyay, S., Marcy, G. W., et al. 2009, *ApJ*, 693, 1084
- Zucker, S., & Mazeh, T. 2001, *ApJ*, 562, 549

Appendix A: Additional material

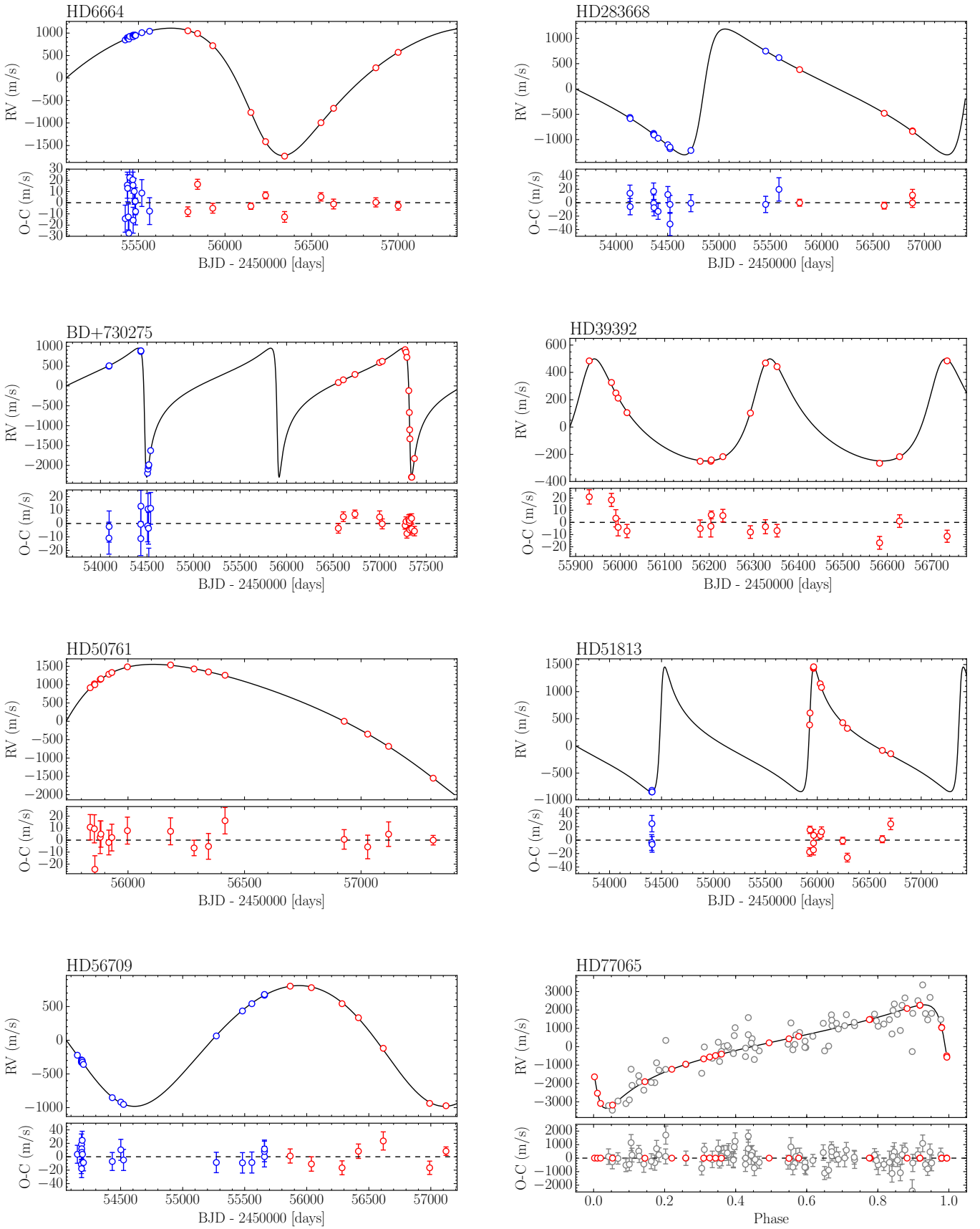


Fig. A.1. Radial velocity measurements obtained with SOPHIE. *The top panel shows the best fit to the data with the bottom panel showing the best fit residuals.* Blue points indicate data taken prior to the 17th of June 2011 instrument upgrade. The grey points represent data from Latham et al. (2002).

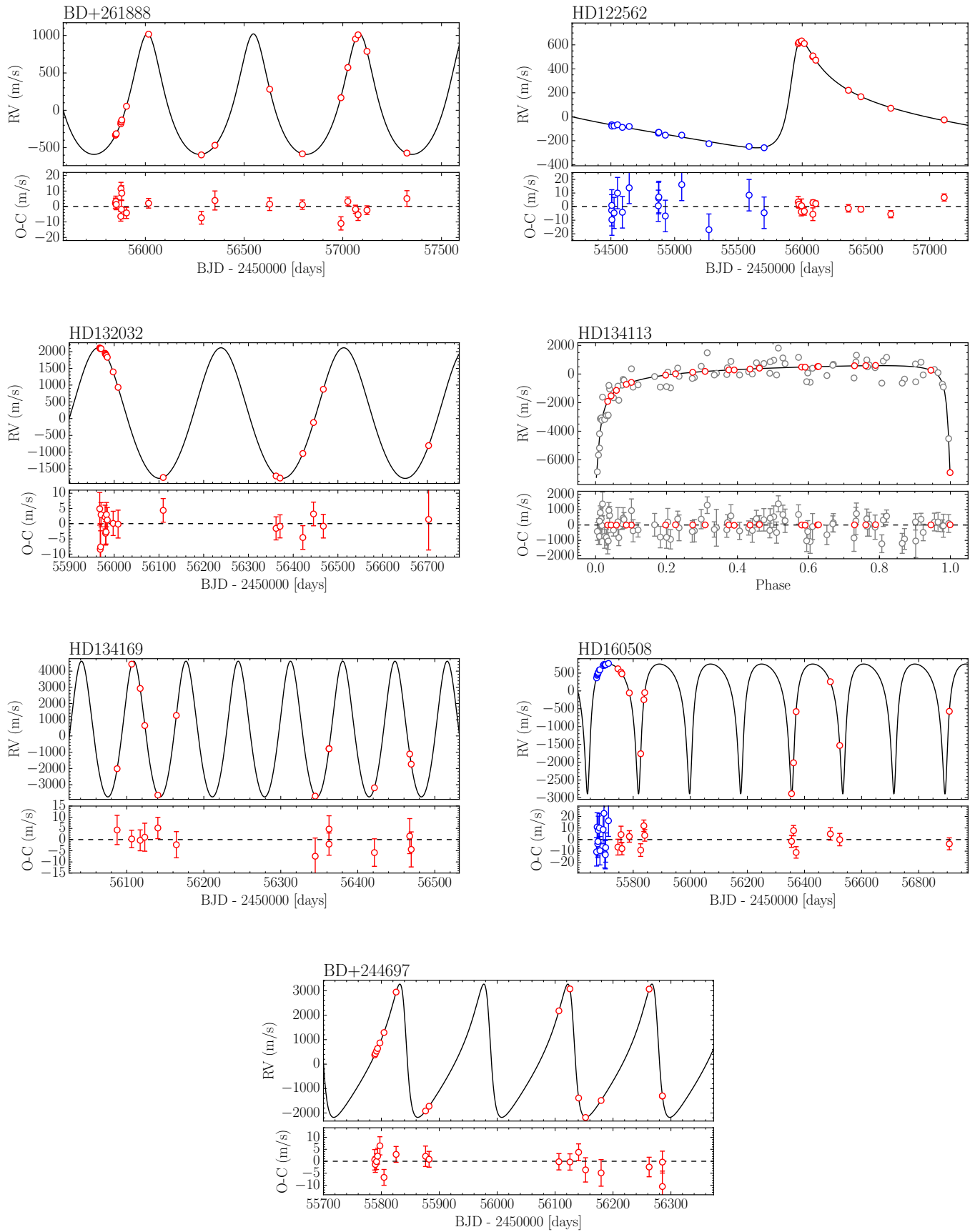


Fig. A.1. continued.

Table A.1. Brown dwarf candidates to solar-type stars with (projected) masses between 10 and 80 M_{Jup} and periods $<10^5$ days.

Name	m_2 [M_{Jup}]	$m_2 \sin i$ [M_{Jup}]	Period [days]	Eccentricity	M_\star [M_\odot]	T_{eff} [K]	$\log g$ [cgs]	[Fe/H] [dex]	R_p/R_\star	SpT	Reference
BD+24 4697b		53 ± 3	145.081 ± 0.016	0.50048 ± 0.00043	0.75 ± 0.05	5077 ± 32	4.67 ± 0.07	-0.11 ± 0.02		K2	1
BD+26 1888b		26 ± 2	536.78 ± 0.25	0.2675 ± 0.0016	0.76 ± 0.08	4748 ± 87	4.3 ± 0.2	0.02 ± 0.04		K7	1
BD+48 2155b		62.6 ± 0.6	90.2695 ^{+0.0188} _{-0.0187}	0.4375 ± 0.0040	1.11 ± 0.08	6004 ± 34	4.53 ^{+0.15} _{-0.13}	0.04 ± 0.06		G0	2
CoRoT-15b	63.3 ± 4.1		3.06036 ± 0.00003	0 (fixed)	1.32 ± 0.12	6350 ± 200	4.3 ± 0.2	0.1 ± 0.2	1.12 ^{+0.30} _{-0.15}	F7V	3
CoRoT-27b	10.39 ± 0.55		5.81943 ± 0.00006	<0.065	1.05 ± 0.11	5900 ± 120	4.4 ± 0.1	-0.1 ± 0.1	0.0990 ± 0.0020	G2	4
CoRoT-33b	59.0 ^{+1.8} _{-1.7}		5.819143 ± 0.000018	0.0700 ± 0.0016	0.86 ± 0.04	5225 ± 80	4.4 ± 0.1	0.44 ± 0.10	0.12 ± 0.04	G9V	5
CoRoT-3b	21.7 ± 1.0		4.25680 ± 0.00001	0 (fixed)	1.37 ± 0.09	6740 ± 140	4.22 ± 0.07	-0.02 ± 0.06	1.01 ± 0.07	F3V	6
G 268-114b / HIP 5158b		15.04 ± 10.55	9017.76 ± 3180.74	0.14 ± 0.10	0.780 ± 0.021	4962 ± 89	4.37 ± 0.20	0.10 ± 0.07		K5V	7
HAT-P-13c		14.28 ± 0.28	446.27 ± 0.22	0.6616 ± 0.0054	1.32 ± 0.20	5640 ± 90	4.13 ± 0.04	0.41 ± 0.08		G4	8, 9, 10
HD 106270b		11.0 ± 0.8	2890 ± 390	0.402 ± 0.054	1.320 ± 0.092	5638 ± 44	3.90 ± 0.06	0.08 ± 0.03		G5	11
HD 114762b		10.99 ± 0.09	83.9152 ± 0.0028	0.3325 ± 0.0048	0.83 ± 0.01	5673 ± 44	4.135 ± 0.060	-0.774 ± 0.030		F9V	12, 13, 14, 15, 16
HD 122562b		24 ± 2	2777 ⁺¹⁰⁴ ₋₈₁	0.71 ± 0.01	1.13 ± 0.13	4958 ± 67	3.74 ± 0.14	0.31 ± 0.04		G5	1
HD 131664b	23 ⁺²⁶ ₋₅		1951 ± 41	0.638 ± 0.020	1.10 ± 0.03	5886 ± 21	4.44 ± 0.10	0.32 ± 0.02		G3V	17, 18
HD 132032b		70 ± 4	274.33 ± 0.24	0.0844 ± 0.0024	1.12 ± 0.08	6035 ± 33	4.45 ± 0.05	0.22 ± 0.03		G5	1, 19
HD 13507b		67 ⁺⁸ ₋₉	4890 ⁺²⁰⁹ ₋₁₈₅	0.20 ± 0.04	1.050 ± 0.150	5755 ± 44	4.56 ± 0.06	0.00 ± 0.03		G0	1, 14, 20
HD 136118b	42 ⁺¹¹ ₋₁₈		1188 ± 2	0.34 ± 0.01	1.24 ± 0.07	6097 ± 44	4.05 ± 0.06	-0.050 ± 0.030		F9V	13, 14, 21, 22, 23
HD 137510b	27.3 to 59.5	27.3 ± 1.9	801.30 ± 0.45	0.3985 ± 0.0073	1.36 ± 0.04	6131 ± 50	4.02 ± 0.04	0.38 ± 0.13		G0 IV	13, 14, 24, 25
HD 14348b		48.9 ± 1.6	4740 ⁺⁶ ₋₅	0.455 ± 0.004	1.10 ± 0.08	6237 ± 47	4.51 ± 0.07	0.28 ± 0.03		F5V	26
HD 14651b		47.0 ± 3.4	79.4179 ± 0.0021	0.4751 ± 0.0010	0.96 ± 0.03	5491 ± 26	4.45 ± 0.03	-0.04 ± 0.06		G6	25
HD 156846b		10.57 ± 0.29	359.5546 ± 0.0071	0.84785 ± 0.00050	1.35 ± 0.05	5969 ± 44	3.92 ± 0.08	0.17 ± 0.04		G0V	27, 28
HD 160508b		48 ± 3	178.9049 ± 0.0074	0.5967 ± 0.0009	1.25 ± 0.08	6212 ± 30	4.16 ± 0.03	0.01 ± 0.02		F8V	1
HD 162020b		14.4	8.428198 ± 0.000056	0.277 ± 0.002	1.450 ± 0.240	4845 ± 44	4.90 ± 0.06	0.00 ± 0.03		K3V	13, 29
HD 16760b		13.13 ± 0.56	466.47 ± 0.35	0.084 ± 0.003	0.78 ± 0.05	5629 ± 44	4.47 ± 0.06	0.067 ± 0.050		G5V	30, 31
HD 167665b		50.6 ± 1.7	4451.8 ^{+27.6} _{-27.3}	0.340 ± 0.005	1.14 ± 0.03	6224 ± 50	4.44 ± 0.10	-0.05 ± 0.06		F9	13, 32, 33
HD 168443c		34 ± 9	1749.83 ± 0.57	0.2113 ± 0.0017	0.995 ^{+0.019} _{-0.050}	5491 ± 44	4.07 ± 0.06	0.04 ± 0.03		G6IV	29, 35, 36, 37
HD 174457b		65.8	840.80 ± 0.05	0.23 ± 0.01	1.030 ± 0.170	5852 ± 44	4.08 ± 0.06	-0.15 ± 0.03		F8	14, 38
HD 189310b		25.6 ^{+0.9} _{-0.8}	14.18643 ± 0.00002	0.359 ± 0.001	0.83 ± 0.02	5188 ± 50	4.49 ± 0.1	-0.01 ± 0.06		K2V	33
HD 190228b		49.4 ± 14.8	1136.1 ± 9.9	0.531 ± 0.028	1.821 ± 0.050	5348 ± 44	3.98 ± 0.06	-0.25 ± 0.03		G5IV	13, 20, 22, 35, 39
HD 191760b		38.17 ± 1.02	505.65 ± 0.42	0.63 ± 0.01	1.28 ^{+0.02} _{-0.10}	5821 ± 82	4.13 ^{+0.05} _{-0.04}	0.29 ± 0.07		G3IV	33, 40
HD 202206b		17.5	256.20 ± 0.03	0.433 ± 0.001	1.180 ± 0.200	5788 ± 44	4.49 ± 0.06	0.31 ± 0.03		G6V	13, 29, 41
HD 209262b		32.3 ^{+1.6} _{-1.5}	5431 ⁺¹³⁵ ₋₉₅	0.347 ^{+0.010} _{-0.008}	1.02 ± 0.07	5815 ± 28	4.41 ± 0.04	0.10 ± 0.02		G5V	26
HD 211847b		19.2 ± 1.2	7929.4 ^{+1999.1} _{-2500.2}	0.685 ^{+0.068} _{-0.067}	0.94 ± 0.04	5715 ± 50	4.49 ± 0.10	-0.08 ± 0.06		G5V	33
HD 217786b		13.0 ± 0.8	1319 ± 4	0.40 ± 0.05	1.02 ± 0.03	5966 ± 65	4.35 ± 0.11	-0.135 ± 0.043		F8V	42
HD 219077b		10.39 ± 0.09	5501 ⁺¹³⁰ ₋₁₁₉	0.770 ± 0.003	1.05 ± 0.02	5362 ± 18	4.00 ± 0.03	-0.13 ± 0.01		G8V+	43
HD 22781b		13.65 ± 0.97	528.07 ± 0.14	0.8191 ± 0.0023	0.75 ± 0.03	5027 ± 50	4.60 ± 0.02	-0.37 ± 0.12		K0	25
HD 283668b		53 ± 4	2558 ± 8	0.577 ± 0.011	0.68 ± 0.06	4845 ± 66	4.35 ± 0.12	-0.75 ± 0.12		K3V	1
HD 30246b		55.1 ^{+20.3} _{-8.2}	990.7 ± 5.6	0.838 ± 0.081	1.05 ± 0.04	5833 ± 44	4.39 ± 0.04	0.17 ± 0.10		G1	25
HD 30339b		77.8	15.0778 ± 0.0003	0.25 ± 0.01	1.580 ± 0.330	6074 ± 44	4.37 ± 0.06	0.21 ± 0.03		F8V	13, 38

References. (1) This work ; (2) Jiang et al. (2013); (3) Bouchy et al. (2011b); (4) Parviainen et al. (2014); (5) Csizmadia et al. (2015); (6) Deleuil et al. (2008); (7) Feroz et al. (2011); (8) Winn et al. (2010); (9) Bakos et al. (2009); (10) Southworth et al. (2012); (11) Johnson et al. (2011); (12) Latham et al. (1989); (13) Valenti & Fischer (2005); (14) Butler et al. (2006); (15) Haywood (2008); (16) Kane et al. (2011a); (17) Sozzetti & Desidera (2010); (18) Moutou et al. (2009); (19) Latham et al. (2002); (20) Perrier et al. (2003); (21) Fischer et al. (2002); (22) Wittenmyer et al. (2009a); (23) Martioli et al. (2010); (24) Endl et al. (2004); (25) Diaz et al. (2012); (26) Bouchy et al. (2016); (27) Tamuz et al. (2008); (28) Kane et al. (2011b); (29) Udry et al. (2002); (30) Sato et al. (2009); (31) Bouchy et al. (2007); (32) Patel et al. (2007); (33) Sahlmann et al. (2011b); (34) Marcy et al. (2001); (35) Zucker & Mazeh (2001); (36) Reffert & Quirrenbach (2006); (37) Pilyavsky et al. (2011); (38) Nidever et al. (2002); (39) Sivan et al. (2004); (40) Jenkins et al. (2009); (41) Correia et al. (2005); (42) Moutou et al. (2011); (43) Marmier et al. (2013); (44) Fischer et al. (2003); (45) Wright et al. (2009); (46) Benedict et al. (2010); (47) Santos et al. (2005); (50) Sahlmann et al. (2011a); (51) Santos et al. (2010); (52) Duquennoy & Mayor (1991); (53) Halbwachs et al. (2000); (54) Wittenmyer et al. (2009b); (55) Siverd et al. (2012); (56) Bouchy et al. (2011a); (57) Bonomo et al. (2015); (58) Siverd et al. (2012); (59) Bonucki et al. (2011); (60) Ford et al. (2011); (61) Diaz et al. (2013); (62) Moutou et al. (2013); (63) Ranc et al. (2015); (64) Ma et al. (2013); (65) Kane et al. (2009); (66) Fleming et al. (2012); (67) Fleming et al. (2010); (68) Hellier et al. (2009); (69) Triand et al. (2010); (70) Anderson et al. (2011); (71) Johns-Krull et al. (2008); (72) Winn et al. (2008); (73) Hébrard et al. (2008); (74) Winn et al. (2009).

Table A.1. continued.

Name	m_2 [M_{Jup}]	$m_2 \sin i$ [M_{Jup}]	Period [days]	Eccentricity	M_* [M_{\odot}]	T_{eff} [K]	$\log g$ [cgs]	[Fe/H] [dex]	R_p/R_*	SpT	Reference
HD 38529c	$17.6^{+1.5}_{-1.2}$	13.99 ± 0.59	2136.14 ± 0.29	0.362 ± 0.002	$1.34^{+0.02}_{-0.05}$	5674 ± 40	3.94 ± 0.12	0.40 ± 0.05		G4V	13, 22, 34, 36, 44, 45, 46
HD 39091b / * pi. Men b		10.27 ± 0.84	2151 ± 85	0.6405 ± 0.0072	1.118 ± 0.088	5950 ± 44	4.36 ± 0.06	0.04 ± 0.03		G0V	13, 15
HD 39392b		13.2 ± 0.8	$394.3^{+1.4}_{-1.2}$	0.394 ± 0.008	1.08 ± 0.08	5951 ± 42	4.08 ± 0.03	-0.32 ± 0.03		F8	1
HD 4747b		$39.6 - 58.1$	$7900 - 29000$	$0.676 - 0.831$	0.81 ± 0.02	5316 ± 50	4.48 ± 0.1	-0.21 ± 0.05		G8	13, 33, 38, 47
HD 52756b		$59.3^{+2.0}_{-1.9}$	52.8657 ± 0.0001	0.6780 ± 0.0003	0.83 ± 0.01	5216 ± 65	4.47 ± 0.11	0.13 ± 0.05		K1V	33
HD 5388b	69.2 ± 19.9	1.96	777.0 ± 4.0	0.40 ± 0.02	1.21 ± 0.12	6297 ± 32	4.28 ± 0.06	-0.27 ± 0.02		F6V	50, 51
HD 72946b		60.4 ± 2.2	5814.45^{+55}_{-1026}	0.495 ± 0.006	0.96 ± 0.07	5656 ± 40	4.5 ± 0.06	0.11 ± 0.03		G5V	26
HD 77065b		41 ± 2	$119.1135^{+0.0026}_{-0.0027}$	0.69397 ± 0.00036	0.75 ± 0.06	4990 ± 100	4.28 ± 0.20	-0.51 ± 0.10		G	1, 19
HD 89707b		$53.6^{+7.8}_{-6.9}$	298.5 ± 0.1	$0.900^{+0.039}_{-0.035}$	0.96 ± 0.04	6047 ± 50	4.52 ± 0.10	-0.33 ± 0.06		G1V	33, 52, 53
HD 91669b		30.6 ± 2.1	497.5 ± 0.6	0.448 ± 0.002	$0.914^{+0.018}_{-0.087}$	5185 ± 87	4.48 ± 0.20	0.31 ± 0.08		K0/K1	54
HD 92320b		59.4 ± 4.1	145.402 ± 0.013	0.3226 ± 0.0014	0.92 ± 0.04	5664 ± 24	4.48 ± 0.03	-0.10 ± 0.06		G1	25
KELT-1b	$27.23^{+0.50}_{-0.48}$		1.217513 ± 0.000015	$0.0100^{+0.0100}_{-0.0070}$	1.335 ± 0.063	6516 ± 49	$4.736^{+0.017}_{-0.025}$	0.052 ± 0.079	$0.07806^{+0.00061}_{-0.00058}$	Mid-F	55
Kepler-39b	$20.1^{+1.3}_{-1.1}$		21.087210 ± 0.000037	0.112 ± 0.057	$1.29^{+0.06}_{-0.03}$	6350 ± 100	4.25 ± 0.06	0.10 ± 0.14	$0.0910^{+0.00068}_{-0.00068}$	F7V	56, 57
KOI-205b	$40.8^{+1.7}_{-1.5}$		11.720126 ± 0.000011	<0.015	$0.96^{+0.03}_{-0.04}$	5400 ± 75	4.558 ± 0.014	0.18 ± 0.12	0.09906 ± 0.000094	K0	58, 59, 60, 61
KOI-415b	62.14 ± 2.69		166.78805 ± 0.00022	0.698 ± 0.002	0.94 ± 0.06	5810 ± 80	4.5 ± 0.2	-0.24 ± 0.11	$0.0649^{+0.0017}_{-0.0013}$	G0IV	62
MOA-2007-BLG-197Lb	41 ± 2				0.82 ± 0.04						63
TYC 2087-255-1b		40.0 ± 2.5	9.0090 ± 0.0004	0.226 ± 0.011	1.16 ± 0.08	5903 ± 42	4.07 ± 0.16	-0.23 ± 0.04		G0IV	64
TYC 2534-698-1b		39.1 ± 11.5	103.698 ± 0.111	0.385 ± 0.011	0.998 ± 0.040	5700 ± 80	4.5 ± 0.1	-0.25 ± 0.06		G2V	65
TYC 2930-872-1b		68.1 ± 3.0	2.430420 ± 0.000006	0.0066 ± 0.0010	1.21 ± 0.08	6427 ± 33	4.52 ± 0.14	-0.04 ± 0.05		F8	66
TYC 2949-557-1b		64.3 ± 3.0	5.69459 ± 0.000029	$0.0017^{+0.0019}_{-0.0015}$	1.25 ± 0.09	6135 ± 40	4.4 ± 0.1	0.32 ± 0.01		F	67
WASP-18b	$10.11^{+0.24}_{-0.21}$		$0.94145290^{+0.0000078}_{-0.0000086}$	$0.00848^{+0.00085}_{-0.00095}$	1.24 ± 0.04	6400 ± 100	4.4 ± 0.2	0.00 ± 0.09	$0.09576^{+0.00105}_{-0.00063}$	F6	68, 69
WASP-30b	60.96 ± 0.89		4.156736 ± 0.000013	0 (fixed)	1.166 ± 0.026	6201 ± 97	4.280 ± 0.010	-0.03 ± 0.10	0.07057 ± 0.01304	F8V	70
XO-3b	11.79 ± 0.59		3.1915239 ± 0.0000068	0.260 ± 0.017	1.213 ± 0.066	6429 ± 100	4.244 ± 0.041	-0.177 ± 0.080	0.92 ± 0.04	F5V	71, 72, 73, 74